Letter to the Editor

Old title: A new module for trace gas emissions in ICON-ART 2.0: A sensitivity study focusing on acetone emissions and concentrations

New title: An emissions module for ICON-ART 2.0: Implementation and simulations of acetone

M. Weimer, J. Schröter, J. Eckstein, K. Deetz, M. Neumaier, G. Fischbeck, L. Hu, D. B. Millet, D. Rieger, H. Vogel, B. Vogel, T. Reddmann, O. Kirner, R. Ruhnke, and P. Braesicke

Dear Dr Folberth,

Thank you for editing our manuscript. Please find below our point-by-point responses to the referees' comments along with a marked-up version of the changes in the manuscript. The relevant changes include:

1. Due to the comments of both referees we have adapted the title of the manuscript to: "An emissions module for ICON-ART 2.0: Implementation and simulations of acetone"
2. Based on the comments of both referees we have included a paragraph in the introduction describing the methods for emissions used in other atmospheric chemistry models
3. We have rewritten Sect. 3.1.3 due to the comments of both referees and included a sensitivity study by varying $n_{\mathrm{lev,emi}}$ as requested by Referee #1
4. We have included a new figure describing the influence of LAI on online emissions in more detail based on a comment of Referee #2 (Sect. 3.2)
5. Due the comment of Referee #2 we have included ground-based measurements of acetone and compare our simulations with them (Sect. 5 and 7.1) and have added Dr Lu Hu (University of Montana) and Prof Dylan Millet (University of Minnesota) as co-authors of the manuscript
6. We have extended Fig. 12 by the simulations with LAI_{sun} and discussed them in Sect. 7.3
7. We have included Fig. 1 in our responses to Referee #1 in the supplement of the paper.

Kind regards and on behalf of all co-authors,
M. Weimer

Answer to comment of referee #1

A new module for trace gas emissions in ICON-ART 2.0: A sensitivity study focusing on acetone emissions and concentrations

M. Weimer, J. Schröter, J. Eckstein, K. Deetz, M. Neumaier, G. Fischbeck, L. Hu, D. B. Millet, D. Rieger, H. Vogel, B. Vogel, T. Reddmann, O. Kirner, R. Ruhnke, and P. Braesicke

Dear referee,

Thank you for your review of the paper. In the following, you can find our answers to your comments which are in red. When we talk about the "concentration" we mean the "number concentration" (in number of molecules per volume unit), just to clarify the used expressions. In addition, we have changed the variable name of the number of model layers of the emissions from k_{emi} to $n_{\mathrm{lev,emi}}$ and we refer to this number several times in our responses.

1 General comments

Emissions of gas phase tracers, in particular surface emissions, can be brought into the model by at least three methods: (*i*) as a flux condition at the surface to vertical diffusion. In that case, a net flux on the surface is calculated by adding the dry deposition flux. The vertical diffusion distributes the tracer in the boundary layer. (*ii*) as a source term in the chemical kinetic equations in some appropriate model layers. (*iii*) as a tendency in some appropriate model layers near the surface. The authors chose method (*iii*) but should discuss the other methods also which are all associated with a certain operator splitting.

Since we aim to follow the process splitting strategy of ICON (Rieger et al., 2015) we decided not to include emissions according to method (ii). Method (i) can only be used for one of the physics packages of ICON: Either the physics package for numerical weather prediction (NWP) or for climate projections (ECHAM physics). In case of method (iii) the algorithm for including the emissions follows the process splitting strategy as well as it is compatible with both the NWP and the ECHAM physics package.

Nevertheless, we performed a sensitivity test by including the emission mass fluxes in the NWP turbulence scheme. If the same variables are used as input, methods (i) and (iii) differ below $0.1\,\%$ and therefore are equivalent if the emissions are included into the lowest model layer, see Figure 1 herein.

We added the following sentence in Section 3: "Because of our aim to follow the process splitting concept of ICON (Rieger et al., 2015) and in order to be compatible with ICON for both numerical weather prediction and climate projections the emission mass flux densities are converted to volume mixing ratio and added to the tracer volume mixing ratios."

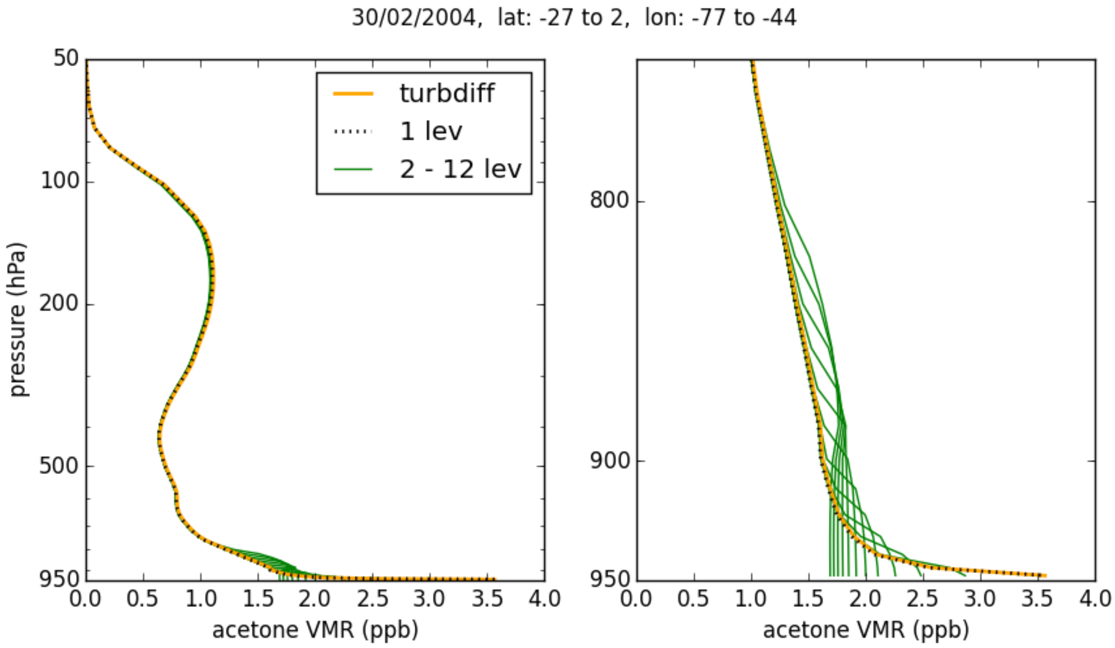

Figure 1: Spatially averaged profiles of the acetone VMR for different methods: adding emission fluxes to vertical turbulent diffusion (orange), method described in paper for $n_{\text{lev,emi}} = 1$ (emission height of $20\,\text{m}$, black dotted) and 2 to 12 (emission height of $65\,\text{m}$ to $\sim 1500\,\text{m}$ above ground, green thin lines).

What concerns me most is the fact that the criteria are unclear according to which the number of lowermost layers are chosen into which the emissions are brought as a tendency.

We have added a paragraph in Section 3.1.3 including Figure 1 in this answer. In this new paragraph, we describe that we select $n_{\text{lev,emi}} = 1$ because the shown profiles are nearly identical above the height of around $750\,\text{hPa}$. Since our aim in the paper is the simulation of acetone in the UTLS region our results should be robust against other choices of $n_{\text{lev,emi}}$.

Our change in the manuscript:

"To investigate the differences in changes of $n_{\text{lev,emi}}$ we perform sensitivity simulations of acetone by varying $n_{\text{lev,emi}}$ between 1 and 12. These simulations are based on constL(megan-offl), see Sect. 6. In Figure 5, profiles of the acetone VMR are shown for the different choices of $n_{\text{lev,emi}}$.

In the case of $n_{\text{lev,emi}} = 1$, no emissions are included in the layers above. For larger values of $n_{\text{lev,emi}}$ the VMR in the lowermost model layer decreases subsequently since the emissions are distributed into a larger column.

Above the specified emission height, all profiles converge each other and above around $750\,\text{hPa}$ the influence of varying $n_{\text{lev,emi}}$ is negligible. Because of our aim to simulate acetone in the UTLS region, the choice of $n_{\text{lev,emi}}$ should make no difference. That is why we simply select $n_{\text{lev,emi}} = 1$ for all used offline emissions."

The authors should discuss this choice, prepare an appropriate sensitivity study varying the number of levels and perform a simulation with emissions given as a flux condition to the vertical diffusion equation.

We have done that (see above and Figure 1 herein).

In this latter simulation, the resulting tendencies in the lowermost model layers should be compared with the number of model layers used in method (*iii*). It would be particularly interesting to see the seasonal variation.

As described above, we could show that both methods are equivalent. To avoid confusion, we focus on the method that has been chosen as the default implementation for ICON-ART.

Discuss other chemistry general circulation models and what methods they use

We have increased the introduction section of the paper with respect to this:
"Different approaches to include emissions in atmospheric modelling have been developed in the past and are used in current chemistry climate models: In the limited area chemistry model WRF-chem (Grell et al., 2005) emissions are treated as production terms in the chemical equations (McKeen et al., 1991). Emissions can be prescribed as a flux condition in the vertical diffusion, as e.g. in the Community Atmosphere Model (Lamarque et al., 2012; Neale et al., 2013) which is part of the Community Climate System Model (CCSM, Gent et al., 2011). This method is also used for emissions in the planetary boundary layer in the GEOS-Chem model (Bey et al., 2001) including the HEMCO module (Keller et al., 2014). Emissions in higher altitudes are brought into GEOS-Chem as a tendency in the respective height of the emissions (C. A. Keller, pers. comm., 2017). The MESSy interface (Jöckel et al., 2005) incorporated e.g. in the EMAC model (Jöckel et al., 2006) gives the possibility to choose the used method for including emissions into the model: Either emissions are prescribed as flux condition as described above or the increase of the tracer mixing ratio is calculated and added to the tracer (Kerkweg et al., 2006). The latter method is also used in the coupled limited area model COSMO-ART (COSMO: COnsortium for SMall-scale MOdelling, ART: Aerosols and Reactive Trace Gases, Vogel et al., 2009)."

2 Specific comments

p.2, l.26: The ICON model is not really "in development" anymore since the NWP physics is used for operational weather forcast.

We have rephrased this sentence:
"ICON is a non-hydrostatic atmospheric model developed with the aim of providing a global model for both weather and climate (Wan et al., 2013; Zängl et al., 2015). Since January 2016, it is operationally used for global numerical weather prediction at German Weather Service (DWD). In July 2016, ICON also replaced the limited area model COSMO-EU (Baldauf et al., 2011) by a nested area over Europe."

p.3, Tab.1: The "official ICON grid number": Give a citation here.

We have cited the web site where the global grids currently can be downloaded from: http://icon-downloads.zmaw.de/dwd_grids.xml
On this web site, the grids are called "official" grids.

p.3, l.1: It should be clarified that Leuenberger et al. generalized the SLEVE coordinates

We have done that.

p.3, l.5 ff: The usual definition of volume mixing ratios is moles tracer per moles dry air. In ICON, tracers are defined per moist air for the horizontal transport. How do you treat these different definitions? How did you check mass conservation?

We have reformulated Eqs. (2) and (3) so that it should be clear that the moles of air are calculated by the ideal gas law using pressure and temperature values of ICON. As these equations are then independent of the explicit molar mass of the air, the moles of the air are that of moist air.
With respect to the second question: The mass conservation of the tracers in ICON was discussed by Zängl et al. (2015). Since ICON-ART uses the ICON tracer structure to calculate the tracers this is also valid for ICON-ART.

The conversion to VMR in Sect. 3.1.3 is now formulated in the paper as follows (of course with other equation numbers):
"Generally, the VMR is defined as fraction of the number of moles of the tracer (in our case the number of moles of the emission Δn_i) and the number of moles of (moist) air n_{air}:

$$\Delta X_{\text{emi},i} = \frac{\Delta n_i}{n_{\text{air}}} \tag{1}$$

The moles of the emission are calculated as the emission mass flux density E_i multiplied by the advective model time step Δt and the base area A of the grid box and divided by the molar mass of the species M_i:

$$\Delta n_i = \frac{E_i \, A \, \Delta t}{M_i} \tag{2}$$

The emission flux can be included into one or more lowest model levels to be specified in the LaTeX table, see Fig. 3. In the following, we will refer to this number as $n_{\text{lev,emi}}$. The total number of model layers is stated as n_{lev}. In ICON, the lowest model layer has the highest index so that the index of the lowest model layer is $l = n_{\text{lev}}$. For calculating the number of moles of the air we sum up the moles of air of the lowest $n_{\text{lev,emi}}$ model layers using the ideal gas law:

$$n_{\text{air}} = \sum_{l=n_{\text{lev}}-n_{\text{lev,emi}}+1}^{n_{\text{lev}}} n_{\text{air},l} = \sum_{l=n_{\text{lev}}-n_{\text{lev,emi}}+1}^{n_{\text{lev}}} \frac{p_l \, V_l}{R^* \, T_l} = \frac{A}{R^*} \sum_{l=n_{\text{lev}}-n_{\text{lev,emi}}+1}^{n_{\text{lev}}} \frac{p_l \, h_l}{T_l} \tag{3}$$

Accordingly, p_l, T_l, h_l and R^* stand for pressure, temperature and geometric height of the grid box and the universal gas constant, respectively.
With Eqs. (2) and (3) the VMR tendency of the emission $\mathrm{d}X_{\mathrm{emi},i}/\mathrm{d}t$, which is added to the tracer, is calculated according to:"

$$\frac{\mathrm{d}X_{\mathrm{emi},i}}{\mathrm{d}t} \approx \frac{\Delta n_i}{n_{\mathrm{air}}\,\Delta t} = \frac{E_i\,R^*}{M_i} \cdot \left(\sum_{l=n_{\mathrm{lev}}-n_{\mathrm{lev,emi}}+1}^{n_{\mathrm{lev}}} \frac{p_l\,h_l}{T_l} \right)^{-1} \tag{4}$$

p.5, Fig.2: "reset simulation year from boundary year back to current year": It's not so clear what you mean here. You would like to say that the last year for which emissions are given is repeated for all years later than this year. By the way, this may even be error prone repeating the last year without warning.

We have adapted the figure accordingly. In the ICON output a message is given for each file that is read so that the user is able to trace which files are used during runtime.

p.6, l.10: Emissions are interpolated by a nearest neighbour interpolation. A flux conserving interpolation would sound more natural since you like to have the same amount of tracer going into the atmosphere irrespective of the used horizontal model resolution. Discuss this.

We have investigated the total mass fluxes of the emissions for different resolutions. The global mass fluxes differ below $1\,\%$.
We have included the following sentence in the manuscript: "This method also conserves the total emission fluxes reasonably with a maximum deviation of 1 % in case of R2B04 and a less deviation for the other resolutions of Table 1 (not shown)."

p.6, l.14: "for each time step" may sound like model time step here, but you mean times for which emissions are provided. Please, rephrase.

We have done that: "Therefore the emission data have to be split into separate files according to their validity time."

p.7, Fig. 3: Lines are cut and not completely displayed.

That it is why it is called "extract" in the figure description. In addition, the important part, i.e. the tracer emission metadata, is shown completely.

p.7, l.5: Fig. 3 shows LATEX not TEX code.

We have replaced TeX by LaTeX.

p.7, l.6: "the number of emission": is it emission sectors, emission types? Be more specific.

We wanted to say "the number of emission types". We have included this word in the paper.

p.7, l.7: "...account only the number..." an "if" is missing. "...is then used globally": Explain better that "the number" is then a globally applied emission mass flux.

We have rephrased this sentence: "The standard value is taken into account only if the number of emission types is zero. Then it is used as the globally applied emission mass flux density. Otherwise [...]"

p.8, l.2: "emission date" may be misinterpreted as the date when emissions are applied (actually, they are applied in every time step), but "emission date" refers to the date for which emission fluxes are provided. Please, rephrase.

We have rephrased this sentence: "The first task of the module during runtime is to find the two dates closest to the simulation time where emission are available in the dataset."

p.8, l.9: Just a remark: Is it necessary to have such a fixed time limit of 11 years? Volcanic emissions could be very irregular, farther away than 11-years and should not be interpolated?

The module was created for the treatment of gas phase emissions from emission inventories. The used value of about 11 years is an arbitrarily chosen stop criterion that is far beyond the time resolution of commonly used inventories such as MACCity, MEGAN-MACC and GFED3. Volcanic emissions are treated in another way in ICON-ART (Rieger et al., 2015).

p.8, l.13: "After interpolation the emission is converted to VMR $(C_{\mathrm{emi,i}})$: Rephrase "emission" to "emission flux"; furthermore, you mean a VMR tendency here, the symbol c is normally used for molarity, so $dX_{\mathrm{emi,i}}/dt$ would be the correct symbol. Devide eq. (2) by time.

We have included "flux" and reformulated Eq. (2) with respect to this (see above).

p.8, eq.(2): In mathematics, sums are not counting backwards. [...]

We have changed that.

p.9, l.1: Explain the choice of k_{emi} in more detail.

We have included a paragraph discussing this choice (see above in our answers to the General Comments).

p.9, l.5: Websites are not a good reference in general. If necessary, add in a footnote the date when you accessed the sites the last time. Similarly: p. 9, l. 15, p. 11, l. 25, p. 16 the footnote, p. 22, l. 3/5

We have done that and where possible we have given another citation.

p.11, l.17: Avoid to start a sentence with a mathematical symbol, in particular when it repeats the symbol of the last sentence

We have adapted this sentence.

p.11, l.28: "derived" instead of "defined".

We have changed that.

p.12, l.6: "sunlit leaves" instead of "sun leaves"

We are aware that the notions "sun leaves" and "sunlit leaves" have different meanings: The term "sunlit leaves" (and "shaded leaves") is used for expressing that vegetation is either directly lit by sun or shaded by other vegetation, which is also used by Dai et al. (2004). The discrimination between "sun leaves" and "shade leaves" is a botanical discrimination.
We actually used the same terms as Dai et al. (2004, "sunlit leaves") and Guenther et al. (2012, "sun leaves") in the paper.

In the manuscript we now consistently follow the naming given by Dai et al. (2004) and rephrased the sentence:
"For standard conditions, we use the average Photosynthetic Photon Flux Density (PPFDS) of the values given by Guenther et al. (2012): $\mathrm{PPFDS} = 125\,\mu\mathrm{mol\,m^{-2}\,s^{-1}}$."

p.13, fig.6: Explain better how you calculate the means. First, the word "global" is irritating, since you are calculating means over "S-America"? In fact, you calculated means over a rectangle in longitude and latitude with sea points contributing to the surface but not to the emissions.

We have excluded the global means from this figure and included a table with the global mass fluxes (now Table 5 in the paper).

p.15, l.7: "...due to Reactions (R5) and (R6)" you probably like to say that (R5) is the rate-determining step.

Yes, we do. We have included this in the paper:
"Reaction 5 results in a cascade of fast reactions and finally in a production of CO and is the largest source for atmospheric CO (Jacob, 1999; Boucher et al., 2001; Seinfeld and Pandis, 2012,

pp. 46–47). Since Reaction 5 is the reaction with lowest reaction rate of this cascade the chemical production of CO can be estimated as follows:"

p.17, l.20: ICON contains several time steps, which one do you mean?

In the documentation of ICON, it is called the "advective" time step which is equivalent to the time step of the fast physics (see Rieger et al., 2015). We have adapted this in the paper where we previously referred to the "model time step".

p.17, l.20: Output interval of 23 hours, meaning output at 0h, 23h (of next day), 22h (of next day), 21h (of next day), and so on?

Yes, that is right. Please see next comment for an explanation.

p.18, l.1: Temporal variability of OH at which time scale?

If the output interval is e.g. daily, we can only investigate OH concentrations at e.g. 00 UTC. However, the OH concentration strongly depends on the daily cycle and therefore also the compounds corresponding to the OH mechanism. That is why we chose an output interval less than daily.

We have adapted the sentence:
"All the simulations include an output interval of 23 hours. With this interval, we are able to see the impact of OH on acetone at different times of day without using too many resources."

p.19, l.15/20/Fig. 8: OH-chem(off): Better choose OH-chem(megan-off) or similar acronyms to make clear that it is not the OH-chemistry being switched off. Fig. 8: Show the free troposphere in an additional panel such that the interannual variability becomes visible.

We have adapted the simulation names to e.g. constL(megan-offl) and OH-chem(megan-onl).
With respect to Figure 8: The interannual acetone lifetime in the free troposphere only differs by 1.7 days in the maximum. That is why we think that the current figure is appropriate for the paper and no additional figure is needed.

p.19, l.12 ff: Your reasons for the underestimation are pure hypotheses and more confusing than explaining your results. The reader is lost what refers to your simulations and what is speculation. Make it clear where your considerations are general and what concerns your situation.

We have reconsidered our first argument because only the second and third ones of the listing are based on literature. Additionally, we have rephrased the remaining sentences:

"(1) We account for chemical production of acetone due to reaction of propane with OH but neglect the contribution of minor VOCs such as monoterpenes. The high impact of monoterpenes on acetone calculated by Khan et al. (2015) was recently challenged by Brewer et al. (2017). On the other hand, we neglect the weak uptake of acetone by the oceans and dry deposition which would decrease the acetone VMR slightly (Fischer et al., 2012; Khan et al., 2015). (2) [...]"

p.20, fig.9: Remove unnecessary axis and titles of the plots. Create one color bar for all panels instead. Instead of a pressure range, give the geometric altitude of the tropopause.

We have adapted the figure accordingly. As described in the text on p.19, l.5-7 the pressure range given in the figures refers to the pressure range where measurement data is considered.
We have added this information to the figure description.

p.20, l.3ff: Describe your result first, then interpret/explain

Due to a new sensitivity simulation, we have adapted the whole paragraph and included a description of the figure:
"The acetone VMR around the tropopause using MEGAN-Online LAI is shown in the rightmost column of Fig. 12."

p.20, l.13: Acetone life time of 1.5 years versus 28 days? This is worth an explanation.

The main difference between these two values lies in their region and time scales they represent: The value of 28 days is a global annual mean value whereas the lifetime of 1.5 years stands for the northern winter mid-latitudinal average (35 to 75 °N).
In contrast to the global average, the low sun during (northern) winter decreases the photolysis rates related to OH and acetone in the mid-latitudes by one to two orders of magnitude. As the acetone loss rate in our simplified model is proportional to these photolysis rates, its lifetime increases accordingly.
We have included this sentence after p.20, l.13: "This value is a mid-latitudinal (35 to 75° N) average for the months December to February in 2005 to 2015 in contrast to the global annual average mentioned above."

p.21, l.5 ff: The conclusions should contain information about the choice of k_{emi} and the sensitivity studies versus a flux condition in vertical diffusion.

We have added a paragraph in the conclusions describing our choice of $n_{\mathrm{lev,emi}}$:

"[...] the number of lowest model levels of the emission $n_{\mathrm{lev,emi}}$ has to be specified where we show a sensitivity test by varying this number. Differences only occur in the height of the emission itself.

Therefore, the tracer mixing ratio above the emission height $n_{\text{lev,emi}}$ is independent of the choice of $n_{\text{lev,emi}}$. Since our focus in the results is the comparison to measurements in the upper troposphere and lowermost stratosphere (UTLS), we choose $n_{\text{lev,emi}} = 1$."

p.22, l.1-5: Code availability: give a contact person only since there seems to be no icon license available at the site given (address not found!). The ART license is referring to a person anyhow.

We have adapted the code availability paragraph by giving contact persons.

Appendix A: "Concentration" should be either "molarity" or "number concentration" since concentration can be anything, mole fraction, volume mixing ratios, molality, molonity and the like. It's confusing to have a species index and a time step index on c in the same section. Put $c_{i,t}(x)$ where x refers to the location, i to the species and t is time. Write the equations for an arbitrary integration step from t to $t + \Delta t$. From (A2) on you can, if you like, omit the index i. Mark the various solutions with superscripts $^{(e)}$ for explicit Euler and $^{(pc)}$ for the predictor-corrector method.

We have clarified the expression concentration and adapted the indices of c: "We here refer to 'concentration' as an abbreviation of number concentration."

p.23, l.9: Better: "If Δt becomes larger than...". What do you mean with "unstable"?

We now give an example in the paper where we assume the chemical production P in Eq. (A6) to be zero, i.e.: $P_* = P_n = 0$ and additionally $\tau_* + \tau_n - \Delta t < 0$. In this case, the concentration of the next time step c_{n+1} becomes negative which obviously shows that the numerical solution does not converge the physical solution of the differential equation.

p.27, l.8: Give the page in Pandis/Seinfeld.

We have added it for each citation in the main text.

3 technical corrections

We have corrected all the technical mistakes.

References

Baldauf, M., Seifert, A., Förstner, J., Majewski, D., Raschendorfer, M., and Reinhardt, T.: Operational Convective-Scale Numerical Weather Prediction with the COSMO Model: Description and Sensitivities, Mon. Weather Rev., 139, 3887–3905, doi:10.1175/MWR-D-10-05013.1, 2011.

Bey, I., Jacob, D. J., Yantosca, R. M., Logan, J. A., Field, B. D., Fiore, A. M., Li, Q., Liu, H. Y., Mickley, L. J., and Schultz, M. G.: Global modeling of tropospheric chemistry with assimilated meteorology: Model description and evaluation, J. Geophys. Res.: Atmospheres, 106, 23 073–23 095, doi:10.1029/2001JD000807, 2001.

Boucher, O., Haigh, J., Hauglustaine, D., Haywood, J., Myhre, G., Nakajima, T., Shi, G., and Solomon, S., eds.: *Radiative Forcing of Climate Change. In:* Climate Change 2001: The Scientific Basis. Contribution of Working Group I to the Third Assessment Report of the Intergovernmental Panel on Climate Change, Cambridge University Press, Cambridge, United Kingdom and New York, NY, USA, 2001.

Brewer, J. F., Bishop, M., Kelp, M., Keller, C., Ravishankara, A. R., and Fischer, E. V.: A sensitivity analysis of key natural factors in the modeled global acetone budget, J. Geophys. Res.: Atmospheres, doi:10.1002/2016JD025935, 2016JD025935, 2017.

Dai, Y., Dickinson, R., and Wang, Y.: A Two-Big-Leaf Model for Canopy Temperature, Photosynthesis, and Stomatal Conductance, J. Clim., 17, 2281–2299, doi:10.1175/1520-0442(2004)017<2281:ATMFCT>2.0.CO;2, 2004.

Fischer, E., Jacob, D. J., Millet, D., Yantosca, R. M., and Mao, J.: The role of the ocean in the global atmospheric budget of acetone, Geophys. Res. Lett., 39, doi:10.1029/2011GL050086, L01807, 2012.

Gent, P. R., Danabasoglu, G., Donner, L. J., Holland, M. M., Hunke, E. C., Jayne, S. R., Lawrence, D. M., Neale, R. B., Rasch, P. J., Vertenstein, M., Worley, P. H., Yang, Z.-L., and Zhang, M.: The Community Climate System Model Version 4, J. Clim., 24, 4973–4991, doi:10.1175/2011JCLI4083.1, 2011.

Grell, G. A., Peckham, S. E., Schmitz, R., McKeen, S. A., Frost, G., Skamarock, W. C., and Eder, B.: Fully coupled online chemistry within the WRF model, Atmos. Environ., 39, 6957–6975, doi:10.1016/j.atmosenv.2005.04.027, 2005.

Guenther, A., Jiang, X., Heald, C., Sakulyanontvittaya, T., Duhl, T., Emmons, L., and Wang, X.: The Model of Emissions of Gases and Aerosols from Nature version 2.1 (MEGAN2.1): an extended and updated framework for modeling biogenic emissions, Geosci. Model Dev., 5, 1471–1492, doi:10.5194/gmd-5-1471-2012, 2012.

Jacob, D. J.: Introduction to atmospheric chemistry, Princeton Univ. Press, Princeton, NJ, 1st edn., 1999.

Jöckel, P., Sander, R., Kerkweg, A., Tost, H., and Lelieveld, J.: Technical Note: The Modular Earth Submodel System (MESSy) - a new approach towards Earth System Modeling, Atmos. Chem. Phys., 5, 433–444, doi:10.5194/acp-5-433-2005, 2005.

Jöckel, P., Tost, H., Pozzer, A., Brühl, C., Buchholz, J., Ganzeveld, L., Hoor, P., Kerkweg, A., Lawrence, M.-G., Sander, R., Steil, B., Stiller, G., Tanarhte, M., Taraborrelli, D., van Aardenne, J., and Lelieveld, J.: The atmospheric chemistry general circulation model ECHAM5/MESSy1: consistent simulation of ozone from the surface to the mesosphere, Atmos. Chem. Phys., 6, 5067–5104, doi:10.5194/acp-6-5067-2006, 2006.

Keller, C. A., Long, M. S., Yantosca, R. M., Da Silva, A. M., Pawson, S., and Jacob, D. J.: HEMCO v1.0: a versatile, ESMF-compliant component for calculating emissions in atmospheric models, Geosci. Model Dev., 7, 1409–1417, doi:10.5194/gmd-7-1409-2014, 2014.

Kerkweg, A., Sander, R., Tost, H., and Jöckel, P.: Technical note: Implementation of prescribed (OFFLEM), calculated (ONLEM), and pseudo-emissions (TNUDGE) of chemical species in the Modular Earth Submodel System (MESSy), Atmos. Chem. Phys., 6, 3603–3609, doi:10.5194/acp-6-3603-2006, 2006.

Khan, M., Cooke, M., Utembe, S., Archibald, A., Maxwell, P., Morris, W., Xiao, P., Derwent, R., Jenkin, M., Percival, C., Walsh, R., Young, T., Simmonds, P., Nickless, G., O'Doherty, S., and Shallcross, D.: A study of global atmospheric budget and distribution of acetone using global atmospheric model STOCHEM-CRI, Atmos. Environ., 112, 269 – 277, doi:10.1016/j.atmosenv.2015.04.056, 2015.

Lamarque, J.-F., Emmons, L. K., Hess, P. G., Kinnison, D. E., Tilmes, S., Vitt, F., Heald, C. L., Holland, E. A., Lauritzen, P. H., Neu, J., Orlando, J. J., Rasch, P. J., and Tyndall, G. K.: CAM-chem: description and evaluation of interactive atmospheric chemistry in the Community Earth System Model, Geosci. Model Dev., 5, 369–411, doi:10.5194/gmd-5-369-2012, 2012.

McKeen, S. A., Hsie, E.-Y., Trainer, M., Tallamraju, R., and Liu, S. C.: A regional model study of the ozone budget in the eastern United States, J, Geophys. Res.: Atmospheres, 96, 10 809–10 845, doi:10.1029/91JD00052, 1991.

Neale, R. B., Richter, J., Park, S., Lauritzen, P. H., Vavrus, S. J., Rasch, P. J., and Zhang, M.: The Mean Climate of the Community Atmosphere Model (CAM4) in Forced SST and Fully Coupled Experiments, J. Clim., 26, 5150–5168, doi:10.1175/JCLI-D-12-00236.1, 2013.

Rieger, D., Bangert, M., Bischoff-Gauss, I., Förstner, J., Lundgren, K., Reinert, D., Schröter, J., Vogel, H., Zängl, G., Ruhnke, R., and Vogel, B.: ICON-ART 1.0 - a new online-coupled model system from the global to regional scale, Geosci. Model Dev., 8, 1659–1676, doi:10.5194/gmd-8-1659-2015, 2015.

Seinfeld, J. H. and Pandis, S. N.: Atmospheric Chemistry and Physics: From Air Pollution to Climate Change, John Wiley & Sons, 2nd edn., 2012.

Vogel, B., Vogel, H., Bäumer, D., Bangert, M., Lundgren, K., Rinke, R., and Stanelle, T.: The comprehensive model system COSMO-ART - Radiative impact of aerosol on the state of the atmosphere on the regional scale, Atmos. Chem. Phys., 9, 8661–8680, doi:10.5194/acp-9-8661-2009, 2009.

Wan, H., Giorgetta, M. A., Zängl, G., Restelli, M., Majewski, D., Bonaventura, L., Fröhlich, K., Reinert, D., Rípodas, P., Kornblueh, L., and Förstner, J.: The ICON-1.2 hydrostatic atmospheric dynamical core on triangular grids - Part 1: Formulation and performance of the baseline version, Geosci. Model Dev., 6, 735–763, doi:10.5194/gmd-6-735-2013, 2013.

Zängl, G., Reinert, D., Rípodas, P., and Baldauf, M.: The ICON (ICOsahedral Non-hydrostatic) modelling framework of DWD and MPI-M: Description of the non-hydrostatic dynamical core, Quart. J. Roy. Meteor. Soc., 141, 563–579, doi:10.1002/qj.2378, 2015.

Answer to comment of referee #2

A new module for trace gas emissions in ICON-ART 2.0: A sensitivity study focusing on acetone emissions and concentrations

M. Weimer, J. Schröter, J. Eckstein, K. Deetz, M. Neumaier, G. Fischbeck, L. Hu, D. B. Millet, D. Rieger, H. Vogel, B. Vogel, T. Reddmann, O. Kirner, R. Ruhnke, and P. Braesicke

Dear referee,

Thank you for your review of the paper. In the following, you can find our answers to your comments which are in red.

1 General comments

As the title says, the emission module is claimed as the new topic, but readers cannot agree with this. Both the offline and online emission modules employ commonly-used techniques and are nothing new.

We have adapted the title as follows: "An emissions module for ICON-ART 2.0: Implementation and simulations of acetone"

Furthermore, descriptions of the off-line emission module are too technical and not suitable in the main text. I recommend to move most of the descriptions in Section 3.1 to a supplementary document as a sort of manual. Only descriptions of emission inventories used and Fig. 5 may be left in the main text.

As described on the website of GMD, our goal is reproducibility: "[...] ideally, the description should be sufficiently detailed to in principle allow for the re-implementation of the model by others, so all technical details which could substantially affect the numerical output should be described"
In addition, Referee #1 requested an even more detailed description of the module. That is why we think that this section is appropriate for the main text.

Comparing only with IAGOS-CARIBIC is not sufficient and more evaluation analyses are required. The evaluation only with the UT/LS data might be misleading, if the model vertical transport, which is often very uncertain, is wrongly simulated. Surface station data may be available and they should be compared with the simulated values in addition.

We have compared the OH-chem simulations with the surface observations of Hu et al. (2013) and included it in the paper, now Sect. 7.1, and discussed the results.

Furthermore, I cannot understand why the authors limited the IAGOS-CARIBIC data to the mid-latitude UT/LS region. I think tropical data and vertical profiles (if available) are also useful to evaluate the overall performance of the model.

We, of course, agree with this comment in principle. However, there are several issues: Firstly the PTRMS needs some time to stabilise, i.e. the first hour of the measurements after take-off generally is not a reliable measurement. Furthermore the PTRMS is switched off at $\sim 700\,\mathrm{hPa}$ to prevent damage of the turbo molecular pumps during landing.

As a second point, our aim was to create a climatology with a methodology similar to that shown in Jöckel et al. (2016).

Additionally, for a meaningful climatology we need sufficient number of measurement points. As the CARIBIC container is always mounted in Germany (Frankfurt or Munich), then flying to an intercontinental airport and coming back to Germany again, the data coverage over the mid-latitudes is much higher than over the tropics.

Furthermore, one more result with MEGAN-Online LAIsun, which is newly introduced in this study, is needed to be shown in the sensitivity test

We have included this test and have discussed the results in Sect. 7.3:

"As could be expected from Fig. 7, the annual cycles of acetone of constL(megan-onl,LAIsun) and OH-chem(megan-onl,LAIsun) are nearly identical with the respective offline emissions simulation except for slightly higher values in case of the LAIsun simulations. Thus, by parametrising the LAI according to Dai et al. (2004) the online biogenic emissions in ICON-ART are in good agreement with the offline data set MEGAN-MACC."

2 Minor comments

Title: As stated above, "a new module for trace gas emissions" seems inappropriate.

We have adapted the title (see above).

P.1, L.12: Insert a space between "dominated" and "concentrations"

We have changed this.

Introduction: What is the benefit of using ICON for atmospheric chemistry studies? Please discuss about that. Also, other previous studies in which similar icosahedral models (other than ICON) are used for atmospheric chemistry should be cited, for example, Suzuki et al. (2008), Elbern et al. (2010), Niwa et al. (2011), Goto et al. (2015)

We have increased the introductory part with respect to this and included the sentence:
"Recent work also includes the development of chemistry-climate models on icosahedral grids (Suzuki et al., 2008; Elbern et al., 2010; Niwa et al., 2011; Goto et al., 2015; Rieger et al., 2015)."

P.2, L.28: "to to" => "to"

We have changed this.

P.4, L.9: What is the overbar of rho?

It means that the air density is Reynolds-averaged (see Rieger et al., 2015).
We have included it in the paper.

P.8, L.14: I cannot understand the summation in Eq. (2).

We have corrected the equation and explained all the symbols (of course the numbers of the equations herein differ from that used in the paper):

"Generally, the VMR is defined as fraction of the number of moles of the tracer (in our case the number of moles of the emission Δn_i) and the number of moles of (moist) air n_{air}:

$$\Delta X_{\text{emi},i} = \frac{\Delta n_i}{n_{\text{air}}} \tag{1}$$

The moles of the emission are calculated as the emission mass flux density E_i multiplied by the advective model time step Δt and the base area A of the grid box and divided by the molar mass of the species M_i:

$$\Delta n_i = \frac{E_i\, A\, \Delta t}{M_i} \tag{2}$$

The emission flux can be included into one or more lowest model levels to be specified in the LaTeX table, see Fig. 3. In the following, we will refer to this number as $n_{\text{lev,emi}}$. The total number of model layers is stated as n_{lev}. In ICON, the lowest model layer has the highest index so that the index of the lowest model layer is $l = n_{\text{lev}}$. For calculating the number of moles of the air we sum up the moles of air of the lowest $n_{\text{lev,emi}}$ model layers using the ideal gas law:

$$n_{\text{air}} = \sum_{l=n_{\text{lev}}-n_{\text{lev,emi}}+1}^{n_{\text{lev}}} n_{\text{air},l} = \sum_{l=n_{\text{lev}}-n_{\text{lev,emi}}+1}^{n_{\text{lev}}} \frac{p_l\, V_l}{R^*\, T_l} = \frac{A}{R^*} \sum_{l=n_{\text{lev}}-n_{\text{lev,emi}}+1}^{n_{\text{lev}}} \frac{p_l\, h_l}{T_l} \tag{3}$$

Accordingly, p_l, T_l, h_l and R^* stand for pressure, temperature and geometric height of the grid box and the universal gas constant, respectively.
With Eqs. (2) and (3) the VMR tendency of the emission $\mathrm{d}X_{\mathrm{emi},i}/\mathrm{d}t$, which is added to the tracer, is calculated according to:"

$$\frac{\mathrm{d}X_{\mathrm{emi},i}}{\mathrm{d}t} \approx \frac{\Delta n_i}{n_{\mathrm{air}}\,\Delta t} = \frac{E_i\,R^*}{M_i} \cdot \left(\sum_{l=n_{\mathrm{lev}}-n_{\mathrm{lev,emi}}+1}^{n_{\mathrm{lev}}} \frac{p_l\,h_l}{T_l} \right)^{-1} \tag{4}$$

P.9, L.1-2: These sentences are not clear to me.

We have separated the calculation of the number of moles of the emission from Eq. (2) and reformulated these sentences (see above). As can be seen, the number of moles Δn_i is independent of the emission height $n_{\mathrm{lev,emi}}$. We have reformulated the sentence:
"This method conserves mass of the emission since the calculated moles of the emission Δn_i are independent of the choice of $n_{\mathrm{lev,emi}}$ and therefore do not change if $n_{\mathrm{lev,emi}}$ is increased."

P.9, L.9: The biomass burning emission seems duplicated. The MACCity inventory includes biomass burning, while another explicit biomass burning data of GFED is also added.

We actually only use the anthropogenic dataset and have removed the "and biomass burning" in the paper.

P.11, L.7: "leaf area index" => "leaf area index (LAI)" P.11, L.8: Delete "(LAI)" P.11, L.11: "leaf area index" => "LAI"

We have changed that.

P.13, L.5: Why is the online emission so much higher than the offline one, although they are made by the same MEGAN?

The advantage of using online emissions lies in the much higher temporal resolution of the input parameters, in case of MEGAN especially the temperature. Thus, emissions are calculated every model time step in contrast to the offline emissions which usually have a monthly temporal resolution. Therefore, it is clear that differences in the emission output occur.
In addition, our configuration is different from that used by Sindelarova et al. (2014) as described in Sect. 3.1.4 and 3.2. The input parameters and metadata come from another model and we adapted the MEGAN model which is described in Sect. 3.2. Hence, although MEGAN in ICON-ART and in Sindelarova et al. (2014) are based on the same source code of Guenther et al. (2012), its implementation is model-specific.
We have included a new figure where the sensitivity of the MEGAN-Online emissions on LAI is demonstrated and discussed (in Section 3.2 in the paper):

"In order to investigate the influence of the parametrisation of LAI by Eq. (7) we show in Fig. 8 the distributions of LAI and LAI_{sun}, together with its influence on the acetone emission. As expected, large values in LAI (top panel) occur over the Amazon region in South America as well as in Central Africa where also the acetone VMR in Fig. 6 maximises. In addition, the forest areas in the east of Canada, northern Europe and Siberia show large values of the LAI. In these regions, the LAI is in the order of 3 to $6\,\mathrm{m}^2\,\mathrm{m}^{-2}$.

For the used solar zenith angle of $10.3°$, the parametrisation according to Eq. (7) smoothes and reduces the LAI to values around $1\,\mathrm{m}^2\,\mathrm{m}^{-2}$ (Fig. 8B). Only for the less vegetated regions such as desserts (Sahara or Atacama), the distribution of LAI_{sun} shows nearly no response to the parametrisation of Dai et al. (2004).

In the MEGAN model the emission mass flux density is proportional to LAI (Guenther et al., 2012). That is why the resulting emissions in MEGAN-Online (Fig. 8C) depend linearly on the LAI for each shown plant type. The highest sensitivity on LAI can be seen for broadleaves in the tropics. Thus, the parametrisation of the LAI according to Dai et al. (2004) can lead to a reduction of the emission in the order of factor 2 to 3 in these regions.

To conclude, the correct treatment of LAI is crucial to get realistic results of the emissions in MEGAN. The parametrisation according to Dai et al. (2004) leads to emission flux densities in the same order of magnitude as in the offline data set MEGAN-MACC (see Fig. 7). Further investigation of this will be presented in Sect. 7."

P.14, L.4: What of Sander et al. (2011) is used?

We have adapted the sentence: "Cross sections and quantum yields are given in a tabulated form originating from Sander et al. (2011) and interpolated on given pressure and temperature values of Cloud-J."

Section 4.2: Is this reaction method for the stratosphere similar to those of other models?

The OH parametrisation as described in Section 4.1 is only valid for tropospheric conditions. In the paper, we are interested in UTLS acetone which is mainly driven by emissions at the surface. As shown in Fig. 7 (of the non-corrected manuscript) our definition of the UTLS region ranges high enough so that the stratospheric chemistry should not really disturb the simplified OH chemistry mechanism.

P.16, L11: "(IFS)" Please cite a paper and list it in Reference, not describing the URL in the footnote.

We have cited it.

P.16, L.20-P.17,L.1: "The air pressure corresponding …in the CH4 VMR." This reason is not enough for the validity of using 1ppmv CH4 as the threshold.

We have rephrased the whole paragraph to clarify this:

"In Fig. 9, the zonal maximum of the air pressure where CH4 VMR decreases below $1\,\mathrm{ppmv}$ (blue dashed) is illustrated along with the zonal minimum of the WMO tropopause pressure (black solid). Additionally, the zonally averaged VMR of $\mathrm{CH_4}$ at the tropopause is shown (red dotted) which ranges from 1.6 (Sounthern Hemisphere) to $1.68\,\mathrm{ppmv}$ (Northern Hemisphere). Due to its relatively long tropospheric lifetime, $\mathrm{CH_4}$ is well-mixed in the troposphere and the $\mathrm{CH_4}$ VMR does not decrease below $1\,\mathrm{ppmv}$. Above the tropopause, the $\mathrm{CH_4}$ VMR decreases with height because of higher photolysis rates in the stratosphere.

As can be seen in Fig. 9, the lowest height where the $\mathrm{CH_4}$ VMR decreases below $1\,\mathrm{ppmv}$ is clearly above the tropopause so that the OH mechanism is also applied in the lowermost stratosphere."

P.17, L.14: "110 to 261 and 373 to 528" Are they flight numbers? And where did the aircraft fly to? Please clarify.

Yes, they are the CARIBIC flight numbers. We have included a statistic of the destinations of the flights used for the climatologies. It can be found in Appendix B in the paper.

P.17, L.20-21: "All the simulations …in the tracer concentrations" is not clear to me.

If the output interval is e.g. daily, we can only investigate OH concentrations at e.g. 00 UTC. However, the OH concentration strongly depends on the daily cycle and therefore also the compounds corresponding to the OH mechanism. That is why we chose an output interval less than daily.

We have rephrased this sentence: "All the simulations include an output interval of 23 hours. With this interval, we are able to see the impact of OH on acetone at different times of day without using too many resources."

Appendix A: Description of tau is needed somewhere.

We have added it.

References

Dai, Y., Dickinson, R., and Wang, Y.: A Two-Big-Leaf Model for Canopy Temperature, Photosynthesis, and Stomatal Conductance, J. Clim., 17, 2281–2299, doi:10.1175/1520-0442(2004)017<2281:ATMFCT>2.0.CO;2, 2004.

Elbern, H., Schwinger, J., and Botchorishvili, R.: Chemical state estimation for the middle atmosphere by four-dimensional variational data assimilation: System configuration, J. Geophys. Res.: Atmospheres, 115, doi:10.1029/2009JD011953, d06302, 2010.

Goto, D., Dai, T., Satoh, M., Tomita, H., Uchida, J., Misawa, S., Inoue, T., Tsuruta, H., Ueda, K., Ng, C. F. S., Takami, A., Sugimoto, N., Shimizu, A., Ohara, T., and Nakajima, T.: Application of a global nonhydrostatic model with a stretched-grid system to regional aerosol simulations around Japan, Geosci. Model Dev., 8, 235–259, doi:10.5194/gmd-8-235-2015, 2015.

Guenther, A., Jiang, X., Heald, C., Sakulyanontvittaya, T., Duhl, T., Emmons, L., and Wang, X.: The Model of Emissions of Gases and Aerosols from Nature version 2.1 (MEGAN2.1): an extended and updated framework for modeling biogenic emissions, Geosci. Model Dev., 5, 1471–1492, doi:10.5194/gmd-5-1471-2012, 2012.

Hu, L., Millet, D. B., Kim, S. Y., Wells, K. C., Griffis, T. J., Fischer, E. V., Helmig, D., Hueber, J., and Curtis, A. J.: North American acetone sources determined from tall tower measurements and inverse modeling, Atmos. Chem. Phys., 13, 3379–3392, doi:10.5194/acp-13-3379-2013, 2013.

Jöckel, P., Tost, H., Pozzer, A., Kunze, M., Kirner, O., Brenninkmeijer, C. A. M., Brinkop, S., Cai, D. S., Dyroff, C., Eckstein, J., Frank, F., Garny, H., Gottschaldt, K.-D., Graf, P., Grewe, V., Kerkweg, A., Kern, B., Matthes, S., Mertens, M., Meul, S., Neumaier, M., Nützel, M., Oberländer-Hayn, S., Ruhnke, R., Runde, T., Sander, R., Scharffe, D., and Zahn, A.: Earth System Chemistry integrated Modelling (ESCiMo) with the Modular Earth Submodel System (MESSy) version 2.51, Geosci. Model Dev., 9, 1153–1200, doi:10.5194/gmd-9-1153-2016, 2016.

Niwa, Y., Tomita, H., Satoh, M., and Imasu, R.: A Three-Dimensional Icosahedral Grid Advection Scheme Preserving Monotonicity and Consistency with Continuity for Atmospheric Tracer Transport, J. Meteorolog. Soc. Jpn. Ser. II, 89, 255–268, doi:10.2151/jmsj.2011-306, 2011.

Rieger, D., Bangert, M., Bischoff-Gauss, I., Förstner, J., Lundgren, K., Reinert, D., Schröter, J., Vogel, H., Zängl, G., Ruhnke, R., and Vogel, B.: ICON-ART 1.0 - a new online-coupled model system from the global to regional scale, Geosci. Model Dev., 8, 1659–1676, doi:10.5194/gmd-8-1659-2015, 2015.

Sander, S., Abbatt, J., Barker, J., Burkholder, J., Friedl, R., Golden, D., Huie, R., Kolb, C., Kurylo, M., Moortgat, K., Orkin, V., and Wine, P.: Chemical Kinetics and Photochemical Data for Use in Atmospheric Studies, Evaluation No. 17, JPL Publication 10-6, 2011.

Sindelarova, K., Granier, C., Bouarar, I., Guenther, A., Tilmes, S., Stavrakou, T., Müller, J.-F., Kuhn, U., Stefani, P., and Knorr, W.: Global data set of biogenic VOC emissions calculated by the MEGAN model over the last 30 years, Atmos. Chem. Phys., 14, 9317–9341, doi:10.5194/acp-14-9317-2014, 2014.

Suzuki, K., Nakajima, T., Satoh, M., Tomita, H., Takemura, T., Nakajima, T. Y., and Stephens, G. L.: Global cloud-system-resolving simulation of aerosol effect on warm clouds, Geophys. Res. Lett., 35, doi:10.1029/2008GL035449, l19817, 2008.

~~A new~~ An emissions module for ~~trace gas emissions in~~ ICON-ART 2.0: ~~A sensitivity study focusing on acetone emissions~~ Implementation and ~~concentrations~~simulations of acetone

Michael Weimer[1,2], Jennifer Schröter[2], Johannes Eckstein[2], Konrad Deetz[2], Marco Neumaier[2], Garlich Fischbeck[2], Lu Hu[3], Dylan B. Millet[4], Daniel Rieger[2], Heike Vogel[2], Bernhard Vogel[2], Thomas Reddmann[2], Oliver Kirner[1], Roland Ruhnke[2], and Peter Braesicke[2]

[1]Steinbuch Centre for Computing, Karlsruhe Institute of Technology, 76344 Eggenstein-Leopoldshafen, Germany
[2]Institute of Meteorology and Climate Research, Karlsruhe Institute of Technology, 76344 Eggenstein-Leopoldshafen, Germany
[3]University of Montana, Department of Chemistry and Biochemistry, Missoula, MT, 59812, USA
[4]Department of Soil, Water, and Climate, University of Minnesota, Saint Paul, MN, 55108, USA

Correspondence to: M. Weimer (michael.weimer@kit.edu)

Abstract. We present a ~~new~~ recently developed emissions module for the ICON (ICOsahedral Non-hydrostatic)-ART (Aerosols and Reactive Trace gases) modelling framework. The emissions module processes external flux data sets and increments the tracer volume mixing ratios in the boundary layer accordingly. ~~In addition, the module for online calculations of biogenic emissions (MEGAN2.1) is implemented in ICON-ART and can replace the offline biogenic emission data sets.~~

The performance of the emissions module is illustrated with simulations of acetone, using a simplified chemical depletion mechanism based on a reaction with OH and photolysis only.

In our model setup, we calculate a tropospheric acetone lifetime of 33 days, which is in good agreement with the literature. We compare our results with ground-based as well as with airborne IAGOS-CARIBIC measurements in the upper troposphere and lowermost stratosphere (UTLS) in terms of phase and amplitude of the annual cycle. In all our ICON-ART simulations the general seasonal variability is well represented but ~~questions~~ uncertainties remain concerning the magnitude of the acetone emissions~~and its atmospheric lifetime.~~ .

In addition, the module for online calculations of biogenic emissions (MEGAN2.1) is implemented in ICON-ART and can replace the offline biogenic emission data sets. In a sensitivity study we show how different parametrisations of the leaf area index (LAI) change the emission fluxes calculated by MEGAN2.1 and demonstrate the importance of an adequate treatment of the LAI within MEGAN2.1.

We conclude that the ~~new~~ emissions module performs well ~~and~~ with offline and online emission fluxes and allows the simulation of the annual cycles of emissions ~~dominatedconcentrations even with a simple chemistry only.~~

dominated substances.

1 Introduction

Many trace gases (called tracers hereafter) are emitted into the atmosphere by sources located at the Earth's surface. Especially for volatile organic compounds (VOCs), natural and anthropogenic emissions as well as secondary production from emitted precursor compounds are major atmospheric sources (e.g., Blake and Blake, 2002; Atkinson and Arey, 2003).

~~Two different approaches to account for~~ Different approaches to include emissions in atmospheric modelling have been developed in the past ~~: The emission fluxes are either read from external data sets or calculated online with the possibility to account for the current state of the atmosphere in the model (e.g., Kerkweg et al., 2006; Keller et al., 2014)~~and are used in current chemistry climate models: In the limited area chemistry model WRF-chem (Grell et al., 2005) emissions are treated as production terms in the chemical equations (McKeen et al., 1991). Emissions can be prescribed as a flux condition in the vertical diffusion, as e.g. in the Community Atmosphere Model (Lamarque et al., 2012; Neale et al., 2013) which is part of the Community Climate System Model (CCSM, Gent et al., 2011). This method is also used for emissions in the planetary boundary layer in the GEOS-Chem model (Bey et al., 2001) including the HEMCO module (Keller et al., 2014). Emissions in higher altitudes are brought into GEOS-Chem as a tendency in the respective height of the emissions. The MESSy interface (Jöckel et al., 2005) incorporated e.g. in the EMAC model (Jöckel et al., 2006) gives the possibility to choose the used method for including emissions into the model: Either emissions are prescribed as flux condition as described above or the increase of the tracer mixing ratio is calculated and added to the tracer (Kerkweg et al., 2006). The latter method is also used for the MACC reanalysis (Monitoring Atmospheric Composition and Climate, Inness et al., 2013) and in the coupled limited area model COSMO-ART (COSMO: COnsortium for SMall-scale MOdelling, ART: Aerosols and Reactive Trace Gases, Vogel et al., 2009).

Recent work also includes the development of chemistry-climate models on icosahedral grids (Suzuki et al., 2008; Elbern et al., 2010; Ni
The ICOsahedral Non-hydrostatic modelling framework (ICON) has been designed for the simultaneous usage for numerical weather prediction and climate simulations (Zängl et al., 2015). It includes the possibility of local grid refinement (nests) with two-way interaction. Due to its good scaling properties ICON is applicable on high performance computers of the next generation.

In the previous version of the coupled chemistry climate modelling framework ICON-ART, only emissions of aerosols are considered ~~(ICON: ICOsahedral Non-hydrostatic modelling framework, ART: Aerosols and Reactive Trace gases, Rieger et al., 2015; Zän~~
A module accounting for trace gas emissions was not existing so far.

Here we present a ~~new interface~~ module for including emissions from external data sources in ICON-ART which is independent of the temporal resolution of the underlying emission data. This ~~interface~~ module reads emission mass fluxes from data sets, remapped to the unstructured ICON grid, and interpolates them to the ICON-ART simulation time. After conversion to volume mixing ratio (VMR) the ~~emission is~~ emissions are added to the tracer VMR in ICON-ART in the lowest model layers. This number is specified by the user.

In addition, the Model of Emissions of Gases and Aerosols from Nature (MEGAN2.1, Guenther et al., 2012) as implemented in ICON-ART is presented. This model calculates biogenic emissions of VOCs online, i.e. dependent on the current state of the atmosphere.

We also describe a new simplified mechanism for depletion of trace gases due to reaction with OH, the main tropospheric sink for most VOCs (Blake and Blake, 2002). This mechanism allows the space and time dependent calculation of the tracers' loss rate. Thus, these new developments now allow the investigation of VOCs with ICON-ART.

Several VOCs act as precursors of OH and HO_2 ($= HO_x$) radicals particularly in the dryer upper troposphere and lowermost stratosphere (UTLS) (Folkins and Chatfield, 2000). HO_x can deplete ozone so that VOCs have climatic impact in the UTLS region (e.g., Neumaier et al., 2014). In this study, we will focus on the influence of acetone which is together with methanol one the most abundant VOC in the UTLS region. Mixing ratios of $300 - 2000\,\mathrm{pptv}$ ($1\,\mathrm{pptv} = 10^{-12}\,\mathrm{mol\,mol^{-1}}$) have been observed in the Northern Hemisphere ~~midlatitudes~~ mid-latitudes (Singh et al., 1995; Jaeglé et al., 1998; Heikes et al., 2002; Sprung and Zahn, 2010; Elias et al., 2011; Neumaier et al., 2014).

This study is organised as follows: In Sect. 2 the model ICON with its ART extension is described followed by the description of the ~~new emission interface in ICON-ART in~~ emissions module in Sect. 3. Then, the simplified mechanism for VOC depletion is introduced (Sect. 4). After a description of the ~~IAGOS-CARIBIC project~~ used measurements of acetone and the simulations for this study in Sections 5 and 6, the results are presented in Sect. 7 followed by conclusions and an outlook (Sect. 8).

2 The ICON model with its ART extension

In this section, we briefly describe the ICON model (Sect. 2.1) and its ART extension (Sect. 2.2). More detailed descriptions can be found in Zängl et al. (2015) and Rieger et al. (2015), respectively.

2.1 The ICON model

ICON is a non-hydrostatic atmospheric model ~~which is currently under development~~ developed with the aim of providing a global model for both weather and climate (Wan et al., 2013; Zängl et al., 2015). Since January 2016, it is operationally used for global numerical weather prediction at German Weather Service (DWD). In July 2016, ICON also replaced the limited area model COSMO-EU (Baldauf et al., 2011) by a nested area over Europe.

Horizontal discretisation is performed on an icosahedral-triangular C grid. In contrast to ~~to~~ the regular latitude-longitude grid, this is an unstructured grid where the grid points are saved as one-dimensional arrays.

In this study, we use the same resolution notation as introduced by Zängl et al. (2015): RnBk with n and k as indicators for root division and bisections, respectively. Usual resolutions and the corresponding global number of grid cells are shown in Table 1.

In the vertical, generalised smooth-level coordinates as described by Leuenberger et al. (2010) are used (see Fig. 1).

In ICON tracers are transported by solving the continuity equation of mass for each tracer discretised with a time-split method: Finite volume method is used in the vertical whereas a simplified flux-form semi-Lagrangian method is used for horizontal transport (Miura, 2007; Lauritzen et al., 2011; Rieger et al., 2015).

Table 1. Examples of ICON resolutions with characteristic length $\overline{\Delta x}$ and total number of cells (from Zängl et al., 2015). Characteristic length and number of cells are calculated according to $\overline{\Delta x} = \sqrt{\pi/5}\,R/(n\,2^k)$ and $n_c = 20\,n^2\,4^k$ (R = Earth's radius and n and k as ICON resolution indicators). The grid number denotes the official ICON grid number[a] for the grid configuration used in this study, rotated by 36 degrees around z-axis.

resolution	$\overline{\Delta x}$ (in km)	number of cells	grid number
R2B04	157.8	20 480	0012
R2B05	78.9	81 920	0014
R2B06	39.5	327 680	0016
R2B07	19.7	1 310 720	0018
R3B07~~[a]~~[b]	13.9	2 949 120	0022

[a] http://icon-downloads.zmaw.de/dwd_grids.xml (latest access on 10 February 2017)

[b] global operational resolution at DWD

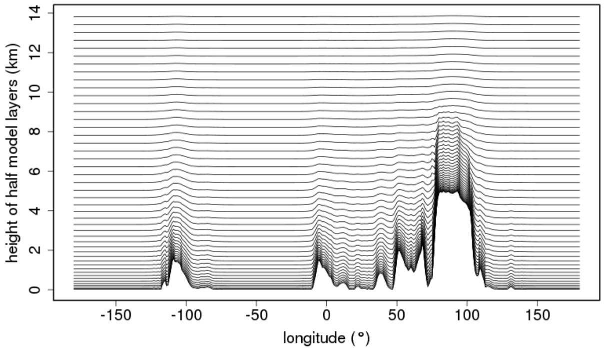

Figure 1. Height of the lowest 46 ICON model layers at ~~33 °~~33° N in the configuration with 90 total model layers.

Current tracers in ICON are water vapour and hydrometeors depending on the chosen microphysics scheme. In this study, the microphysics scheme is based on that used in COSMO ~~(COnsortium for SMall-scale MOdelling, Doms and Schättler, 2004)~~ (Doms and Sc described in the technical documentation as part of the ICON source code (Seifert, 2010).

The tropopause height will play an important role in this study. In our simulations, it is calculated by ICON routines according to the thermal definition of World Meteorological Organization (WMO) (1957).

2.2 The ART module

The ART module for ICON is currently under development with the following aims (Rieger et al., 2015):

- Treatment of aerosols and gas-phase species in global modelling

- Gas-phase and heterogeneous chemistry
- Investigation of the feedbacks between aerosols, trace gases and the state of the atmosphere

Tracers in ICON-ART are transported and diffused in the same way as the internal ICON tracers like water vapour. The ICON-ART tracers used in this study include methane ($\mathrm{CH_4}$), carbon monoxide (CO), propane ($\mathrm{C_3H_8}$) and acetone ($\mathrm{CH_3C(O)CH_3}$).

Chemical reactions are calculated according to the following equation:

$$\frac{\partial \overline{\rho}\hat{\psi}_i}{\partial t} = -A_i + P_i - L_i + E_i \qquad (1)$$

where ~~ρ~~ $\overline{\rho}$, ψ_i, A_i and P_i are Reynolds-averaged air density, partial density fraction, advection and chemical production of the tracer i, respectively. The hat over ψ denotes the barycentric average.

E_i and L_i are emission and loss rate of tracer i, respectively. In version 1.0 of ICON-ART (Rieger et al., 2015), no general algorithm for including E_i was included and the lifetime and therefore L_i was assumed to be globally constant. In version 2.0 used here, we added ~~an interface~~ a module for emissions (see Sect. 3) and a simplified OH chemistry for calculation of the loss rate (see Sect. 4).

Additionally, we implemented the predictor-corrector method according to ~~Seinfeld and Pandis (2012)~~ Seinfeld and Pandis (2012, pp. 11 solve Eq. (1) for tracer depletion via reaction with OH. This method is more accurate than that described by Rieger et al. (2015). A detailed description of the predictor-corrector method can be found in Appendix A.

3 The ~~new~~ emission ~~interface~~ module in ICON-ART

We have included modules for offline and online calculation of emissions in ICON-ART. Both approaches are described in this section. In Section 3.1, we demonstrate our method to read and treat offline emissions whereas the description of the MEGAN2.1 model for online calculation of biogenic emissions in the configuration for ICON-ART follows in Sect. 3.2.

Because of our aim to follow the process splitting concept of ICON (Rieger et al., 2015) and in order to be compatible with ICON for both numerical weather prediction and climate projections the emission mass flux densities are converted to volume mixing ratio and added to the tracer volume mixing ratios.

We also perform a sensitivity study by including the emissions as lower boundary condition in the vertical turbulent diffusion scheme of ICON which can be found in the supplement of the paper. In this figure, we demonstrate that the method used in this study (see Sect. 3.1.3) and the method using the turbulent diffusion are equivalent if the emissions are included into the lowermost model layer ($n_{\mathrm{lev,emi}} = 1$).

3.1 Offline emissions

Offline emissions in ICON-ART are calculated with a new module for including emissions from external data sources which is described in the following. The process can be separated into four steps (see Fig. 2): pre-processing, initialisation, reading and finalisation.

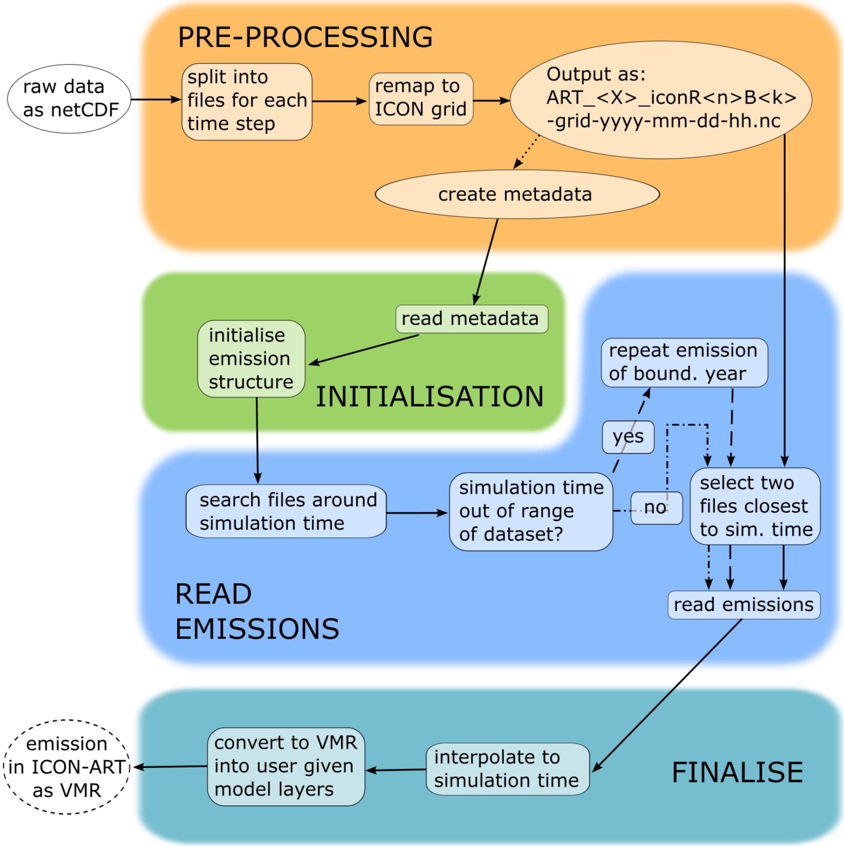

Figure 2. Flow chart of the process from the external netCDF emission data with regular grid and emission data as mass flux density to the emission as VMR in ICON-ART. The process can be separated into four steps: pre-processing, initialisation, read emissions and ~~finalise~~ finalising the ~~interface~~module. Pre-processing before the run of ICON-ART is necessary whereas the other processes are included in ICON-ART. Ellipses depict files while rectangles stand for processes. The different arrow lines illustrate either the interaction with the remapped netCDF data set which has to be performed by the user in the pre-processing step (dotted), the “no” path (dotted and dashed) or the “yes” path (dashed).

Table 2. Notation of the abbreviations used for different types of emissions denoted as X in the name structure of the files together with the corresponding integer value used in ICON-ART.

type	abbreviation	integer value
anthropogenic	ANT	10
biogenic	BIO	11
biomass burning	BBE	12
biogenic online	ONL	13

Pre-processing (Sect. 3.1.1) is required before the model run and includes horizontal interpolation of the input data to the ICON grid as well as preparation of meta information of the data set which is committed to the ~~interface~~ module during initialisation.

The other steps are preformed automatically during ~~operation~~ runtime of the model. In the step for reading emission (Sect. 3.1.2), the closest emission dates are searched and the emissions are interpolated to the current simulation time of ICON-ART. Finally, the temporally interpolated emission mass flux density is converted to VMR and added to the tracer VMR into user given number of model layers (Sect. 3.1.3).

In addition, we briefly describe the offline emission inventories used for this study (Sect. 3.1.4) and demonstrate the performance of the module (see Sect. 3.1.5).

3.1.1 Pre-processing of the input data and initialisation of the module

Due to the unstructured icosahedral grid of ICON (see Sect. 2.1), the usually structured latitude-longitude grid of emission data sets has to be interpolated to the ICON grid. This is managed by tools provided by ~~German Weather Service (DWD)~~ DWD called the DWD ICON tools (Prill, 2016). In general, emissions are spatially highly variable. Therefore, the nearest neighbour interpolation method is applied which reasonably captures the spatial variability of the emissions~~and which~~. This method also conserves the total emission ~~flux reasonably~~ fluxes reasonably with a maximum deviation of $1\,\%$ in case of R2B04 and a less deviation for the other resolutions of Table 1 (not shown).

With the current version of ICON-ART, it is only possible to read files consisting of ~~one~~ a single time step. ~~That is why~~ Therefore the emission data have to be ~~separated into single files for each timestep~~split into separate files according to their validity time.

The files to be read by the emission ~~interface~~ module have to follow the general ICON-ART name convention:

ART_<X>_iconR<n>B<k>-grid-
yyyy-mm-dd-hh_<grid-num>.nc

where <X> characterises the three character abbreviation of the emission type (see Table 2), and <n> and <k> are the ICON resolution indicators in the same format as in Table 1. Additionally, the date of the ~~emission~~ emissions and the grid number (see

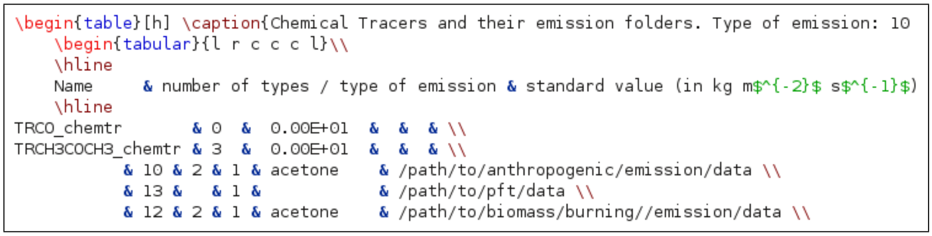

```
\begin{table}[h] \caption{Chemical Tracers and their emission folders. Type of emission: 10
    \begin{tabular}{l r c c c l}\\
    \hline
    Name     & number of types / type of emission & standard value (in kg m$^{-2}$ s$^{-1}$)
    \hline
TRCO_chemtr       & 0  &  0.00E+01  &  &  & \\
TRCH3COCH3_chemtr & 3  &  0.00E+01  &  &  & \\
          & 10 & 2 & 1 & acetone    & /path/to/anthropogenic/emission/data \\
          & 13 &   & 1 &            & /path/to/pft/data \\
          & 12 & 2 & 1 & acetone    & /path/to/biomass/burning//emission/data \\
```

Figure 3. Sample extract of a ~~TeX~~ LaTeX table committing emission metadata to the module. Details see text.

Table 1) are part of the name structure. The maximum temporal resolution of the data set is hourly and every file can include emission data of more than one species.

Emission mass flux densities in units of $\mathrm{kg\,m^{-2}\,s^{-1}}$ are required in the raw data as the values are automatically converted to VMR after the reading process, see Sect. 3.1.3.

The controlling LaTeX table and “first_and_last_date.txt”

~~The controlling TeX table and “first_and_last_date.txt”~~

Some meta information have to be committed to the module, e.g. about the data set’s location on the disk and the variable name in the remapped netCDF file for each emission data set and each tracer in ICON-ART. These metadata are controlled by a ~~TeX~~ LaTeX table (see Fig. ~~??~~3).

In the simplest form, each tracer in the ~~TeX~~ LaTeX table is represented by one line (see tracer CO in Fig. ~~??~~3). This line contains the tracer name (column 1), the number of ~~emissions~~ emission types to be considered (column 2) and the standard value as mass flux density (column 3). ~~This~~ The standard value is taken into account only if the number of ~~emissions is zeroand is then used globally. Then~~ emission types is zero. Then it is used as the globally applied emission mass flux density. Otherwise one line per emission type follows with empty first column, each giving the following:

- column 2: emission type as integer (see Table 2)
- column 3: number of dimensions of the emission data in the file without the time dimension: 2 or 3, for two or three dimensional data
- column 4: number of lowest model layers into which ~~emission~~ the emissions shall be included
- column 5: variable name in the netCDF files
- column 6: full path to the netCDF files

In the example of Fig. ~~??~~3, no emission data sets are considered for CO. Since the standard emission value is set to zero as well, no emissions are computed for CO at all. For acetone, offline and online emissions have to be considered. The

```
1980-01-01T00:00:00Z
2010-12-01T00:00:00Z
```

Figure 4. Content of “first_and_last_date.txt”. It commits the boundary dates of the data set to the module with first date of data set in the first line and last date in the second one. Here, an example is given for the inventory MEGAN-MACC (see Sect. 3.1.4 for further information).

anthropogenic (type is set to 10, see Table 2) and biomass burning data set (type 12) are both two-dimensional emissions to be included in one (i.e. the lowest) model layer and with the variable name “acetone” in the netCDF files. Biogenic emissions in this example are calculated online (type 13). They are also added to the lowest model layer. The path for online emissions refers to the data set of plant functional types (see Sect. 3.2).

If the simulation time exceeds the range of the data set the boundary year is repeated as long as necessary (see Fig. 2 in the “read emission” step). That is why the boundary dates of the data set also have to be committed to the module. For this, the ASCII file “first_and_last_date.txt” placed in the same folder as the data set is used containing the first and the last date of the data set in the ICON date format in separate lines as shown in Fig. 4.

3.1.2 Reading emissions

The first task of the module during ~~operation~~ runtime is to find the two ~~emission~~ dates closest to the simulation time where emissions are available in the dataset. For this, one hour is successively added to or subtracted from the simulation time until a file at that date is found. The next file is searched only if the simulation time exceeds the date of the later emission file.

Apart from limits of the temporal resolution, no further assumptions of the data set’s temporal resolution have to be made. Missing files or variable temporal resolution of the data are possible and taken care of by the model. As mentioned in Sect. 3.1.1, the lower limit of the temporal resolution is hourly. ICON-ART aborts when no file is found before or after 10^5 hours (about $11\,\mathrm{years}$) with a corresponding error message.

3.1.3 Time interpolation of the emissions and conversion to VMR

The maximum temporal resolution of the data is hourly (see Sect. 3.1.1) but the model time steps in ICON-ART are in the order of minutes for resolution R2B04 or below for higher resolutions. Therefore, the emission data is linearly interpolated to the simulation time.

After interpolation the emission mass flux density is converted to VMR~~($C_{\mathrm{emi},i}$) according to:~~

$$C_{\mathrm{emi},i} = \frac{n_i}{n_{\mathrm{air}}} = \frac{E_i\,\Delta t\,R^*}{M_i}\cdot\left(\sum_{l=k_{\mathrm{lev}}}^{k_{\mathrm{lev}}-k_{\mathrm{emi}}-1}\frac{p_l\,h_l}{T_l}\right)^{-1}$$

~~In this equation for one model grid box, the~~ . Generally, the VMR is defined as fraction of the number of moles of the ~~emission n_i of tracer i is divided by~~ tracer (in our case the number of moles of the emission Δn_i) and the number of moles of (moist) air n_{air}~~.~~ :

$$\Delta X_{\mathrm{emi},i} = \frac{\Delta n_i}{n_{\mathrm{air}}} \tag{2}$$

The moles of ~~emission n_i~~ the emission are calculated as the emission mass flux density E_i multiplied by the advective model time step Δt and the base area A of the grid box ~~(cancels out during division with n_{air})~~ and divided by the molar mass of the ~~tracer~~ species M_i~~. The moles of air n_{air} are calculated via air density multiplied by the volume of the grid box (base area A times height h_l) and divided by the molar mass of the air M_{air} which cancels out when replacing the air density with the~~ :

$$\Delta n_i = \frac{E_i\, A\, \Delta t}{M_i} \tag{3}$$

The emission flux can be included into one or more lowest model layers to be specified in the LaTeX table, see Fig. 3. In the following, we will refer to this number as $n_{\mathrm{lev,emi}}$. The total number of model layers is stated as n_{lev}. In ICON, the lowest model layer has the highest index so that the index of the lowest model layer is $l = n_{\mathrm{lev}}$. For calculating the number of moles of the air we sum up the moles of air of the lowest $n_{\mathrm{lev,emi}}$ model layers using the ideal gas law:

$$n_{\mathrm{air}} = \sum_{l=n_{\mathrm{lev}}-n_{\mathrm{lev,emi}}+1}^{n_{\mathrm{lev}}} n_{\mathrm{air},l} = \cancel{\frac{\rho_{\mathrm{air},l}\, A\, h_l}{M_{\mathrm{air}}}} \sum_{l=n_{\mathrm{lev}}-n_{\mathrm{lev,emi}}+1}^{n_{\mathrm{lev}}} \frac{p_l\, V_l}{R^*\, T_l} = \cancel{\frac{p_l\, A\, h_l}{M_{\mathrm{air}}\, R_{\mathrm{air}}\, T_l}} = \frac{A}{R^*} \sum_{l=n_{\mathrm{lev}}-n_{\mathrm{lev,emi}}+1}^{n_{\mathrm{lev}}} \frac{p_l\, h_l}{T_l} \tag{4}$$

Accordingly, p_l, T_l, h_l and R^* ~~in Eqs. and~~ stand for pressure~~and temperature~~ , temperature and geometric height of the grid box and the universal gas constant, respectively. ~~The resulting emission VMR of Eq.~~

With Eqs. (3) and (4) the VMR tendency of the emission $\mathrm{d}X_{\mathrm{emi},i}/\mathrm{d}t$, which is added to the tracer~~VMR in the user specified number of lowest model layers k_{emi}. In Equation , k_{lev} represents the total number of model layers (90 in our configuration of ICON-ART).~~ , is calculated according to:

$$\frac{\mathrm{d}X_{\mathrm{emi},i}}{\mathrm{d}t} \approx \frac{\Delta n_i}{n_{\mathrm{air}}\, \Delta t} = \frac{E_i\, R^*}{M_i} \left(\sum_{l=n_{\mathrm{lev}}-n_{\mathrm{lev,emi}}+1}^{n_{\mathrm{lev}}} \frac{p_l\, h_l}{T_l} \right)^{-1} \tag{5}$$

This method conserves mass of the emission since the calculated moles of the emission Δn_i are independent of the choice of $n_{\mathrm{lev,emi}}$ and therefore do not change if ~~k_{emi}~~ $n_{\mathrm{lev,emi}}$ is increased. The ~~emission is~~ emissions are just distributed in a larger column.

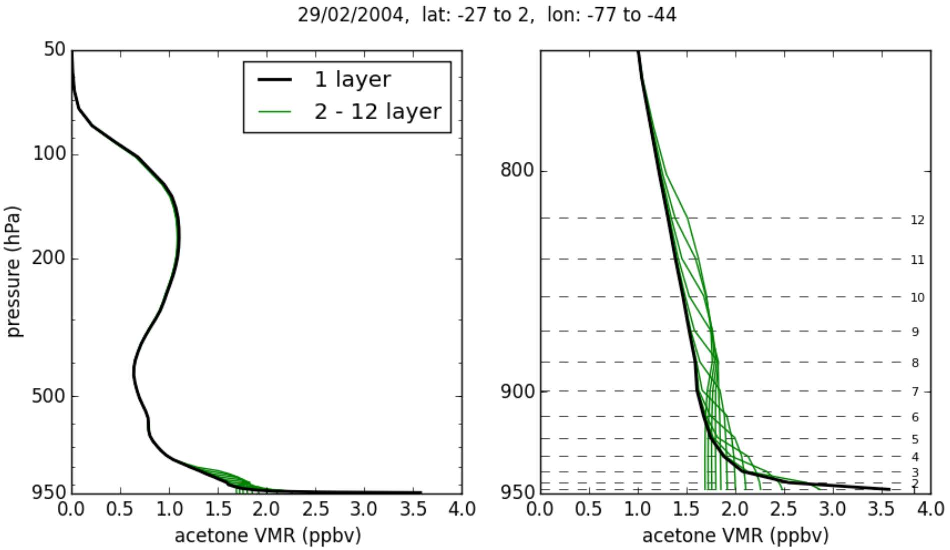

Figure 5. Profiles of the acetone VMR for $n_{\text{lev,emi}} = 1$ (emission height of $20\,\text{m}$ above ground, black thick) and 2 to 12 (emission height of 65 to $\sim 1500\,\text{m}$ above ground, green thin lines) spatially averaged over the Amazon region in Brazil on 29 February 2004, about two months after initialisation. In the right panel, the pressure range is reduced and the average height of the 12 lowest model layers are illustrated by the dashed horizontal lines.

To investigate the differences in changes of $n_{\text{lev,emi}}$ we perform sensitivity simulations of acetone by varying $n_{\text{lev,emi}}$ between 1 and 12. These simulations are based on constL(megan-offl), see Sect. 6. In Figure 5, profiles of the acetone VMR are shown for the different choices of $n_{\text{lev,emi}}$.

In the case of $n_{\text{lev,emi}} = 1$, no emissions are included in the layers above in contrast to $n_{\text{lev,emi}} > 1$. For larger values of $n_{\text{lev,emi}}$ the VMR in the lowermost model layer decreases subsequently since the emissions are distributed into a larger column.

Above the specified emission height, all profiles converge each other and above around $750\,\text{hPa}$ the influence of varying $n_{\text{lev,emi}}$ is negligible. Because of our aim to simulate acetone in the UTLS region, the choice of $n_{\text{lev,emi}}$ should make no difference. That is why we simply select $n_{\text{lev,emi}} = 1$ for all used offline emissions.

3.1.4 Emission inventories

The emission data for the tracers used in this study can be downloaded from the database of Emissions of atmospheric Compounds & Compilation of Ancillary Data (ECCAD, http://eccad.sedoo.fr)[1]. The inventories used for this study are MACCity, EDGARv4.2, MEGAN-MACC and GFED3 and will be described briefly in the following paragraphs. The emission inventories

---

[1] latest access on 10 February 2017

Table 3. Technical details of the emission inventories from ECCAD for tracers in ICON-ART. For abbreviations of the emission types, see Table 2.

inventory	type	time range	resolution		tracers			
			space	time	CH_4	CO	C_3H_8	$CH_3C(O)CH_3$
MACCity[a]	ANT	1960-2020	0.5°	month	-	✓	✓	✓
EDGARv4.2[b]	ANT	1970-2008	0.5°	year	✓	-	-	-
MEGAN-MACC[c]	BIO	1980-2010	0.5°	month	✓	✓	✓	✓
GFED3[d]	BBE	1997-2010	0.5°	month	✓	✓	✓	✓

[a] Lamarque et al. (2010), Diehl et al. (2012), Granier et al. (2011) and van der Werf et al. (2006),
[b] Janssens-Maenhout et al. (2011, 2013), [c] Sindelarova et al. (2014), [d] van der Werf et al. (2010)

are chosen according to length and temporal resolution of the data. A summary of the technical details of each used emission inventory is shown in Table ~~??~~3. This table also shows which inventory is used for which tracer.

The inventory MACCity includes monthly anthropogenic emissions (Granier et al., 2011). The anthropogenic emission data are taken from the historical monthly data set of Atmospheric Chemistry and Climate Model Intercomparison Project (ACCMIP), described by Lamarque et al. (2010), and the Representative Concentration Pathways 8.5 (RCP8.5) emission scenario.

~~The inventory MACCity includes monthly anthropogenic and biomass burning emissions (Granier et al., 2011). The anthropogenic emission data are taken from the historical monthly data set of Atmospheric Chemistry and Climate Model Intercomparison Project (ACCMIP), described by Lamarque et al. (2010), and the Representative Concentration Pathways 8.5 (RCP8.5) emission scenario.~~

In the anthropogenic inventory Emissions Database for Global Atmospheric Research version 4.2 (EDGARv4.2, Janssens-Maenhout et al., 2011, 2013) emissions are calculated with a country-sector method based on emission factors and more than 50 categories of anthropogenic emission sources ~~(for more information see http://edgar. jrc.ec.europa.eu/methodology.php).~~ (for more information see Olivier and Janssens-Maenhout, 2015).

For the inventory MEGAN-MACC (Sindelarova et al., 2014), monthly mean biogenic emissions are calculated with MEGAN2.1 and the same 15 plant functional types as in our configuration (see Sect. 3.2). Meteorological fields are taken from the Goddard Earth Observing System (GEOS) and assimilated to model space. The leaf area index is derived from MODIS retrievals.

Biomass burning emissions in the inventory called Global Fire Emissions Database version 3 (GFED3, van der Werf et al., 2010) are calculated with a modified version of the Carnegie Ames Stanford Approach model ~~(CASA, Field et al., 1995; Potter et al., 1993;~~ Several fire emission types are derived from satellite data and combined for calculating the carbon emission ~~flux~~ fluxes on a monthly basis in each grid cell. The emission ~~flux~~ fluxes for the substances ~~is~~ are calculated using emission factors depending on the type of fire.

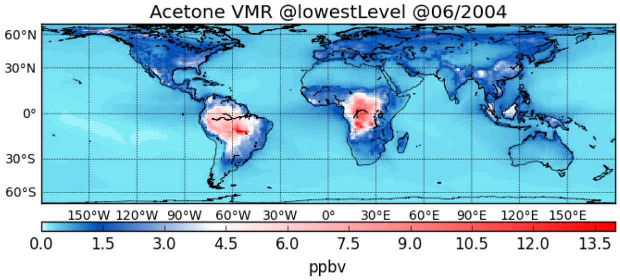

Figure 6. Monthly mean acetone volume mixing ratio in the lowest model layer (layer 90, height of about 20 m above surface) for ~~October 2007~~June 2004, ~~more than 3 years~~ 6 months after initialisation of the ~~constL~~OH-chem(~~off~~megan-offl) simulation (see Sect. 6).

In the used inventories, acetone emissions are dominated by biogenic emissions. Anthropogenic and biomass burning emissions amount for 3 % and 5 % of the total global acetone emission, respectively. These values are consistent with the values published by Jacob et al. (2002) and Fischer et al. (2012).

3.1.5 Performance of the offline module

We demonstrate the performance of the module by including offline emissions for acetone as described in Table ~~??~~3. Figure 6 shows the monthly mean acetone VMR in the lowest model layer for ~~October 2007 for the case of a constant lifetime of .~~ June 2004 in the OH-chem(megan-offl) simulation, see Sect. 6. As biogenic emissions dominate the acetone emissions, the maximum values in the acetone VMR occur over Central Africa and South America where the biogenic emissions of the inventory MEGAN-MACC also are maximised (not shown).

3.2 Online biogenic emissions: MEGAN2.1

To account for the influence of temperature, vegetation and photosynthetically active radiation (PAR) on the ~~emission~~ emissions of acetone, the Model of Emissions of Gases and Aerosols from Nature version 2.1 (MEGAN2.1, MEGAN-Online hereafter) (Guenther et al., 2012) ~~was~~ is implemented into ICON-ART. In contrast to the external acetone data sets (here MEGAN-MACC) which are given as monthly mean values, the online calculation of acetone emissions within Guenther et al. (2012) allows to account for the current conditions in meteorology (especially the diurnal cycle) and vegetation. The parametrisation of biogenic emissions including acetone is described in detail in Guenther et al. (2012), therefore we present here only the main concept of the parametrisation, the changes we have made and the input provided to MEGAN-Online.

MEGAN-Online estimates the biogenic emission mass flux density ~~F~~ E in $\mu\mathrm{g\,m^{-2}\,h^{-1}}$ of the compound class c via the following equation:

$$\underline{F}\underline{E}_c = \gamma_c \sum_j \epsilon_{c,j}\,\chi_j, \tag{6}$$

where $\epsilon_{c,j}$ is the emission factor depending on the vegetation type j with the fractional grid box coverage χ_j. The emission activity factor γ_c accounts for environmental and phenological conditions which affect the emissions.

MEGAN-Online includes 19 compound classes but the study on hand will focus on acetone (~~$c = 13$~~$c = 15$). Guenther et al. (2012) consider the emission affecting processes due to light, temperature, leaf age, soil moisture, leaf area index (LAI) and CO_2 inhibition. The implementation in ICON-ART only accounts for the emission responses from light, temperature, ~~leaf area index (LAI)~~ LAI and leaf age.

The light is provided by ICON-ART as photosynthetically active radiation (PAR) and temperature in the lowest model layer is a standard meteorological variable of ICON-ART. The ~~leaf area index~~ LAI is based on external parameters read during initialisation of ICON-ART. The leaf age considers the fraction of new (FNEW), growing (FGRO), mature (FMAT) and senescing (FSEN) leaves. Due to missing information about the global distribution of these four leaf types, we assumed a uniform distribution. In addition to the standard LAI we have included the parametrisation of Dai et al. (2004) to derive LAI_{sun}, the LAI that is lit by sun ~~, since only this leaf fraction can emit~~ and relevant for the emissions of biogenic VOCs:

$$LAI_{\text{sun}} = \frac{1}{k_b}\Big(1 - \exp\Big(-k_b\, LAI\Big)\Big) \tag{7}$$

with $k_b = G(\mu,\theta)/\mu$. ~~μ is~~ The function $G(\mu,\theta)$ depends on the cosine of the solar zenith angle ~~and $G(\mu,\theta)$ is a function depending on~~ μ and an empirical parameter θ related to the leaf angle distribution. In the following we assume a random distribution of leaf angles which leads to $G(\mu,\theta) = 0.5$ (Dai et al., 2004). The solar zenith angle is provided by ICON-ART. LAI_{sun} was added to MEGAN-Online because Dai et al. (2004) have shown that the net photosynthetic rate of ~~sunlit~~ sun leaves is relatively high due to light saturation whereas a drastic reduction of the photosynthetic rate is visible in the low light layers of shaded leaves. With LAI_{sun} we therefore want to avoid an overestimation of the biogenic emissions especially in areas with high LAI which is linked to a high layering of the leaves (e.g. tropical rain forest).

To consider the vegetation type we use the external plant functional type (PFT) data set provided by ~~the Community Climate System Model (CCSM) (https://svn-ccsm-inputdata.cgd.ucar.edu/trunk/inputdata/lnd/clm2/rawdata/)~~ CCSM (Lawrence and Chase, 2007) 2005 with a grid mesh size of $0.05°$. This PFT data set follows the vegetation class definition of Guenther et al. (2012). The main idea of using PFTs instead of classical vegetation types is to cluster vegetation types with similar biogenic emission characteristics into the same groups for which then the emission factors $\epsilon_{c,j}$ can be ~~defined~~derived.

In addition, MEGAN-Online needs averaged information about PAR and leaf temperature. Highest acetone emissions are observable in tropical regions and therefore we have estimated these values according to this climate zone. The mean Photosynthetic Photon Flux Density (PPFD) over 24 hours (PPFD24) and 240 hours (PPFD240) is estimated to $400\,\mu\text{mol}\,\text{m}^{-2}\,\text{s}^{-1}$ from a simulation study. The mean leaf temperature over 24 hours (T24) and 240 hours (T240) is estimated to 297 K also based on a simulation study. The above mentioned values are not available as regular variables in ICON-ART and therefore have to be estimated (spatiotemporally constant). This could be a further source of uncertainty among the overestimation of the LAI. A sensitivity study by varying 24 and 240 h averages of PAR and leaf temperature results in changes of the emissions

Table 4. Parameters for MEGAN-Online used for this study. Time dependent parameters are written in italic letters.

Variable/Parameter	~~Units~~ Unit	Selection in ICON-ART	Meaning
T	K	Standard ICON-ART output	Temperature at lowest model layer
PAR	$\mathrm{W\,m^{-2}}$	Standard ICON-ART output	Photosynthetically active radiation
SZA	degrees	Standard ICON-ART output	Sun zenith angle
LAI	$\mathrm{m^2\,m^{-2}}$	External data from EXTPAR	Leaf area index
PFT	1	External data from CCSM	Plant functional type
PPFD	$\mathrm{\mu mol\,m^{-2}\,s^{-1}}$	Derived from PAR	Photosynthetic Photon Flux Density
PPFDS	$\mathrm{\mu mol\,m^{-2}\,s^{-1}}$	125	Standard conditions for PPFD averaged over last 24 h
PPFD24	$\mathrm{\mu mol\,m^{-2}\,s^{-1}}$	400	PPFD averaged over last 24 h
PPFD240	$\mathrm{\mu mol\,m^{-2}\,s^{-1}}$	400	PPFD averaged over last 240 h
T24	K	297	Average leaf temperature of the past 24 h
T240	K	297	Average leaf temperature of the past 240 h
FNEW	1	0.25	Fraction of new foliage
FGRO	1	0.25	Fraction of growing foliage
FMAT	1	0.25	Fraction of mature foliage
FSEN	1	0.25	Fraction of senescing foliage
G ~~(μ,θ)~~	1	0.5[a]	function for LAI_{sun} depending on SZA and leaf angle distribution

[a] value given by Dai et al. (2004)

up to 13 % in the maximum for the ranges of 0 to 800 $\mathrm{\mu mol\,m^{-2}\,s^{-1}}$ of PAR and within the temperature range of 283 to 296 K (not shown).

For standard conditions~~the~~, we use the average Photosynthetic Photon Flux Density (PPFDS) ~~is between for shaded leaves and for sun leaves (Guenther et al., 2012). For this study we use the average of~~ of the values given by Guenther et al. (2012): PPFDS = 125 $\mathrm{\mu mol\,m^{-2}\,s^{-1}}$. Table 4 summarises the input of MEGAN-Online and the parameter selection as used for this study.

In the following we compare the results from three emission scenarios: MEGAN-MACC, MEGAN-Online LAI and MEGAN-Online LAI_{sun}. MEGAN-MACC uses the emissions from the external data set. The MEGAN-Online ~~uses~~ scenarios use the online calculated emissions by using LAI (MEGAN-Online ~~LAI~~LAI) and the LAI that is lit by sun (MEGAN-Online LAI_{sun}).

Figure 7 shows the results of the three emission scenarios based on simulations using the numerical weather prediction physics package. The biogenic emission inventory MEGAN-MACC consists of monthly mean values of the MEGAN2.1 model (see Sect. 3.1.4). Therefore, the diurnal cycle is neglected in the inventory. The time series in Fig. 7 are spatially averaged over South America where the global maximum of biogenic emissions occurs, see Fig. 6. The inventory MEGAN-MACC, represented by the ~~black~~ red dashed line in Fig. 7, is linearly interpolated between ~~October and November~~June and

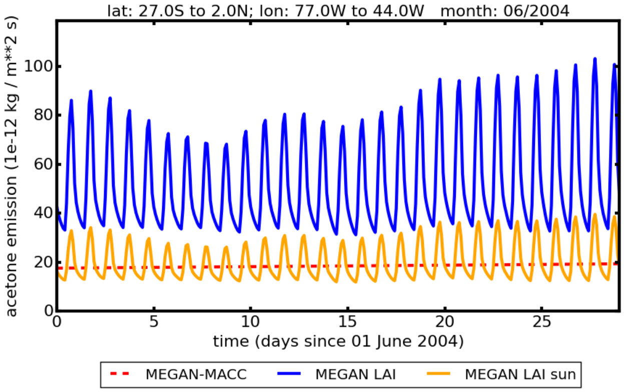

Figure 7. Acetone emission comparison of MEGAN-MACC (black dashed), MEGAN-Online LAI (red) and MEGAN-Online LAI_{sun} (blue) averaged over South America (77 to ~~44 °~~44° W and ~~27 °~~27° S to ~~2 °~~2° N) in ~~October 2007. The mean values represent global means in including the sea where the emissions are zero. The written mean of MEGAN-MACC is the global mean of the first time step in the time series as the MEGAN-MACC emissions already are monthly means.~~ June 2004.

Table 5. Global acetone emission flux F ($\mathrm{Tg\,yr^{-1}}$) for the scenarios of Fig. 7 calculated for the year 2004. Prescribed anthropogenic and biomass burning emissions are included and account for 1.2 and 2.2 $\mathrm{Tg\,yr^{-1}}$, respectively.

scenario	F (in $\mathrm{Tg\,yr^{-1}}$)
MEGAN-MACC	41
MEGAN-Online LAI	92
MEGAN-Online LAI_{sun}	42

July. However, as acetone is emitted as by-product of photosynthesis (Jacob et al., 2002), the diurnal cycle in the emission should be considered.

With online emissions, it is now possible to capture the diurnal cycle in the emissions of acetone. The acetone online emissions are non-zero during the night which is consistent with the literature (e.g., Shao and Wildt, 2002).

The emissions of the MEGAN-Online LAI scenario are more than twice higher than that of MEGAN-MACC. In contrast to this, the emissions due to LAI_{sun} of Eq. (7) have the same global ~~mean~~ flux as MEGAN-MACC (see Table 5), considering the uncertainties in MEGAN-MACC~~).~~. They are also comparable with the emission fluxes mentioned e.g. in Jacob et al. (2002), Fischer et al. (2012), Guenther et al. (2012) and Khan et al. (2015). This means that ~~this parametrisation~~ the parametrisation according to Eq. (7) can be used for investigation of the effect of the diurnal cycle on the emissions and the acetone VMR in the atmosphere.

In order to investigate the influence of the parametrisation of LAI by Eq. (7) we show in Fig. 8 the distributions of LAI and LAI_{sun}, together with its influence on the acetone emission. As expected, large values in LAI (top panel) occur over the

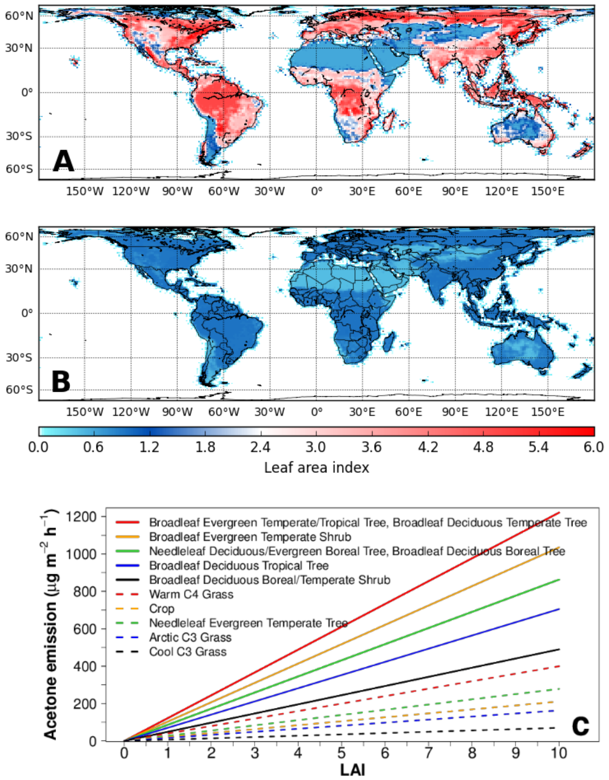

Figure 8. Distribution of (A) LAI in ICON and (B) LAI_{sun} according to Eq. (7) for a solar zenith angle of 10.3°, together with (C) dependence of the acetone emission mass flux density on the LAI for different vegetation types in MEGAN-Online with $T = 300\,\mathrm{K}$ and $PPFD = 400\,\mathrm{\mu mol\,m^{-2}\,s^{-1}}$.

Amazon region in South America as well as in Central Africa where also the acetone VMR in Fig. 6 maximises. In addition, the forest areas in the east of Canada, northern Europe and Siberia show large values of the LAI. In these regions, the LAI is in the order of 3 to $6\,\mathrm{m^2\,m^{-2}}$.

For the used solar zenith angle of 10.3°, the parametrisation according to Eq. (7) smoothes and reduces the LAI to values around $1\,\mathrm{m^2\,m^{-2}}$ (Fig. 8B). Only for the less vegetated regions such as deserts (Sahara or Atacama), the distribution of LAI_{sun} shows nearly no response to the parametrisation of Dai et al. (2004).

In the MEGAN model the emission mass flux density is proportional to LAI (Guenther et al., 2012). That is why the resulting emissions in MEGAN-Online depend linearly on the LAI for each shown plant type (Fig. 8C). The highest sensitivity on LAI can be seen for broadleaf trees in the tropics. Thus, the parametrisation of the LAI according to Dai et al. (2004) can lead to a reduction of the emissions in the order of factor 2 to 3 in these regions.

To conclude, the correct treatment of LAI is crucial to get realistic results of the emissions in MEGAN. The parametrisation according to Dai et al. (2004) leads to emission flux densities in the same order of magnitude as in the offline data set MEGAN-MACC (see Fig. 7). Further investigation of this will be presented in Sect. 7.

4 Parametrisation of tracer depletion with simplified OH chemistry

The main atmospheric sink for VOCs is the reaction with OH. Here, we illustrate the new OH depletion mechanism as implemented in ICON-ART. This parametrisation calculates the ~~tracers' loss rate~~ loss rate of the tracers dependent on space and time and can replace the globally constant lifetime as mentioned in Rieger et al. (2015). As an example, we illustrate the mechanism with acetone as one member of the VOCs.

4.1 Troposphere and UTLS region

As the tracer depletion mechanism by reaction with OH, described below, includes photolysis of ozone we first explain how photolysis rates are treated in ICON-ART.

Photolysis rates in ICON-ART are calculated by the photolysis module which provides precise online calculation of 72 photolytic reactions including an interface between ICON, ICON-ART and the Cloud-J package (Prather, 2015). The impact of clouds and aerosols can be taken into account via different approaches implemented in the module and within Cloud-J. Cloud properties like cloud water path and effective radius of cloud droplets are calculated using ICON micro-physical properties. Cross sections and quantum yields are given in a tabulated form ~~, generated by an interpolation algorithm which uses Sander et al. (2011)~~ originating from Sander et al. (2011) and interpolated on given pressure and temperature values of Cloud-J. The overhead ozone column, that is used, is based on the climatology of Global and regional Earth-system (Atmosphere) Monitoring using Satellite and in-situ data (GEMS, Hollingsworth et al., 2008).

The photolysis module covers roughly the wavelength region from 170 nm up to 850 nm, binned into 18 wavelength bins. Thus, it is possible to accurately calculate photolysis rates from the troposphere up to the stratosphere. For the simulations within this study the average cloud mode of Cloud-J is used.

The tropospheric OH concentration is calculated according to a simplified model, shown e.g. by Jacob (1999), see Reactions (R1) to (R8). In this model, ozone is photolysed producing an oxygen atom in excited state, $\mathrm{O}(^1\mathrm{D})$. $\mathrm{O}(^1\mathrm{D})$ either is quenched by collision with nitrogen ($\mathrm{N_2}$) or oxygen ($\mathrm{O_2}$) or reacts with $\mathrm{H_2O}$, leading to two OH radicals:

$$\mathrm{O_3} + \mathrm{h}\nu \xrightarrow{J_{\mathrm{O_3}}} \mathrm{O}(^1\mathrm{D}) + \mathrm{O_2} \tag{R1}$$

$$\mathrm{N_2} + \mathrm{O}(^1\mathrm{D}) \xrightarrow{k_{\mathrm{N_2}}} \mathrm{O}(^3\mathrm{P}) + \mathrm{N_2} \tag{R2}$$

$$\mathrm{O_2} + \mathrm{O}(^1\mathrm{D}) \xrightarrow{k_{\mathrm{O_2}}} \mathrm{O}(^3\mathrm{P}) + \mathrm{O_2} \tag{R3}$$

$$\mathrm{H_2O} + \mathrm{O}(^1\mathrm{D}) \xrightarrow{k_{\mathrm{H_2O}}} 2\mathrm{OH} \tag{R4}$$

OH is depleted by reaction with either $\mathrm{CH_4}$ or CO, the main sinks for OH (Jacob, 1999):

$$\begin{aligned} \mathrm{OH} + \mathrm{CH_4} &\xrightarrow{k_{\mathrm{CH_4}}} \mathrm{H_2O} + \mathrm{CH_3} && \text{(R5)} \\ &\longrightarrow \cdots \longrightarrow \mathrm{CO} + \mathrm{HO_2} && \text{(R6)} \\ \mathrm{OH} + \mathrm{CO} &\xrightarrow{\mathrm{M}, k_{\mathrm{CO},1}} \mathrm{H} + \mathrm{CO_2} && \text{(R7)} \\ \mathrm{OH} + \mathrm{CO} &\xrightarrow{\mathrm{M}, k_{\mathrm{CO},2}} \mathrm{HOCO} && \text{(R8)} \end{aligned}$$

Reaction rates and photolysis rates in this study are denoted as k and J, respectively. In the following, squared brackets stand for number concentration of the species ~~.~~ (molecules per volume unit). According to the reaction system above, the steady state OH concentration is calculated by the following equation (cf. Jacob, 1999; Dunlea and Ravishankara, 2004; Elshorbany et al., 2016):

$$[\mathrm{OH}] = \frac{2\,[\mathrm{O}(^1\mathrm{D})]\,k_{\mathrm{H_2O}}\,[\mathrm{H_2O}]}{k_{\mathrm{CH_4}}\,[\mathrm{CH_4}] + (k_{\mathrm{CO},1} + k_{\mathrm{CO},2})\,[\mathrm{CO}]} \tag{8}$$

where $[\mathrm{O}(^1\mathrm{D})]$ is calculated by assuming a steady state with Reactions (R1) to (R4) resulting in the following formula:

$$[\mathrm{O}(^1\mathrm{D})] = \frac{J_{\mathrm{O_3}}\,[\mathrm{O_3}]}{k_{\mathrm{O_2}}\,[\mathrm{O_2}] + k_{\mathrm{N_2}}\,[\mathrm{N_2}] + k_{\mathrm{H_2O}}\,[\mathrm{H_2O}]} \tag{9}$$

In Equations (8) and (9), the $\mathrm{O_3}$ photolysis rate $J_{\mathrm{O_3}}$ is calculated by the online photolysis module in ICON-ART (see above in this section). Ozone is provided by the GEMS climatology (Hollingsworth et al., 2008). $[\mathrm{H_2O}]$ is calculated as part of the ICON micro-physics (see Sect. 2.1). $\mathrm{O_2}$ and $\mathrm{N_2}$ VMRs are set to $20.946\,\%$ and $78.084\,\%$, respectively (Brasseur and Solomon, 1995), and converted to number concentrations. The reaction rates in Eqs. (8) and (9) are taken from Sander et al. (2011).

With Equation (8), the loss rates of CO, $\mathrm{CH_4}$ and $\mathrm{C_3H_8}$ are calculated as follows:

$$L_i = k_i\,[\mathrm{OH}], \quad i \in \{\mathrm{CO}, \mathrm{CH_4}, \mathrm{C_3H_8}\} \tag{10}$$

~~A chemical~~ Reaction (R5) results in a cascade of fast reactions and finally in a production of CO ~~due to Reaction is considered in this study (see Reaction) as this reaction is the main~~ and is the largest source for atmospheric CO ~~(Jacob, 1999; Boucher et al.~~ (Jacob, 1999; Boucher et al., 2001; Seinfeld and Pandis, 2012, pp. 46–47). Since Reaction (R5) is the reaction with lowest reaction rate of this cascade the chemical production of CO can be estimated as follows:

$$P_{\mathrm{CO}} = k_{\mathrm{CH4}}\,[\mathrm{OH}]\,[\mathrm{CH_4}] \tag{11}$$

As an example, we will focus on acetone in the following. Acetone is depleted either by reaction with OH or by photolysis where two channels have to be considered:

$$\mathrm{CH_3C(O)CH_3 + OH} \xrightarrow{\mathrm{k_{acetone}}} \mathrm{Products} \tag{R9}$$

$$\mathrm{CH_3C(O)CH_3 + h\nu} \xrightarrow{\mathrm{J_{acetone,1}}} \mathrm{CH_3CO + CH_3} \tag{R10}$$

$$\mathrm{CH_3C(O)CH_3 + h\nu} \xrightarrow{\mathrm{J_{acetone,2}}} \mathrm{2CH_3 + CO} \tag{R11}$$

Reaction (R9) has different channels and is abbreviated here. For the reaction rate k_{acetone}, we use the recommended formula of Sander et al. (2011).

Following Reactions (R9) to (R11), the loss rate of acetone is determined by:

$$L_{\mathrm{acetone}} = k_{\mathrm{acetone}}\,[\mathrm{OH}] + J_{\mathrm{acetone,1}} + J_{\mathrm{acetone,2}} \tag{12}$$

We use the mass-weighted mean shown by SPARC (2013) to calculate the lifetime of acetone:

$$\tau_{\mathrm{acetone}} = \frac{\int [\mathrm{CH_3C(O)CH_3}]\,\mathrm{d}V}{\int L_{\mathrm{acetone}} \cdot [\mathrm{CH_3C(O)CH_3}]\,\mathrm{d}V}\frac{\int [\mathrm{CH_3C(O)CH_3}]\,\mathrm{d}V}{\int L_{\mathrm{acetone}}\,[\mathrm{CH_3C(O)CH_3}]\,\mathrm{d}V} \tag{13}$$

Additionally, the chemical production of acetone due to reaction of propane ($\mathrm{C_3H_8}$) with OH is considered:

$$P_{\mathrm{acetone}} = 0.736\,[\mathrm{C_3H_8}]\,[\mathrm{OH}]\,k_{\mathrm{C_3H_8}} \tag{14}$$

where $k_{\mathrm{C_3H_8}}$ is the reaction rate of $\mathrm{C_3H_8 + OH}$. The value 0.736 is a result of the two channels of this reaction and is taken from Atkinson et al. (2006).

Besides emissions, Eq. (14) is another important source for atmospheric acetone (e.g., Jacob et al., 2002). The acetone production due to other VOCs is neglected.

4.2 Above the UTLS region

The reaction system, described in Sect. 4.1, is valid in the troposphere, only (Jacob, 1999).

In the stratosphere, the lower VMRs of CO and $\mathrm{CH_4}$ in Eq. (8) lead to increases of OH up to $10^8\,\mathrm{molec\,cm^{-3}}$ in the highest model layer (about $2\,\mathrm{Pa}$). According to Brasseur and Solomon (1995), however, the OH number concentration in this altitude is in the order of $10^6\,\mathrm{molec\,cm^{-3}}$. This overestimation of the OH concentration in ICON-ART results in too short lifetimes of the tracers and that is why the lifetime of the species is parametrised in another way for stratospheric conditions.

However, the loss rate of acetone with Eq. (12) is also realistic above the UTLS region due to the photolytic reactions (R10) and (R11).

Therefore, another mechanism is applied above the UTLS region (indicated by the dashed blue line in Fig. 9) only if no other term is added to the loss rate. The lifetime of $\mathrm{CH_4}$ is parametrised pressure-dependent like in the Integrated Forecast

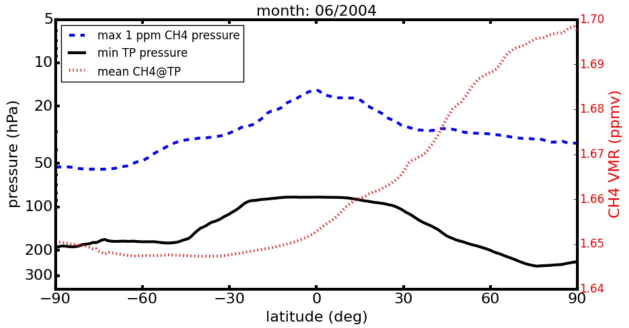

Figure 9. Zonal minimum of tropopause pressure, zonal maximum of 1 ppmv CH_4 pressure and zonal mean of CH_4 VMR at tropopause (right y-axis) for ~~October 2007~~ June 2004 of the OH-chem simulation (see Sect. 6). The 1 ppmv CH_4 pressure in each column is calculated as the air pressure of the model layer where CH_4 VMR decreases below 1 ppmv.

System ~~(IFS)~~[2](IFS, Simmons et al., 1989). In this parametrisation, the CH_4 lifetime in the troposphere is effectively infinite and decreases for pressure below 100 hPa, e.g. it is 2000 days at a pressure of 10 hPa. The CO lifetime is parametrised in the same way as in the KASIMA model (Karlsruhe SImulation model of the Middle Atmosphere) which also depends on pressure, only (Ruhnke et al., 1999; Kouker et al., 1999). The CO lifetime in this parametrisation in an altitude of 100 hPa is about 1 year and in 10 hPa it is 25 days. The formulae of these two lifetime parametrisations have been published by Stassen (2015). The lifetime of propane is set globally to 14 days (Rosado-Reyes and Francisco, 2007).

In order to be able to investigate processes within the UTLS region, a threshold in CH_4 of 1 ppmv $(= 10^{-6}\,\mathrm{mol\,mol^{-1}})$ is applied~~to decide whether~~ . This value ensures the OH mechanism ~~or stratospheric parametrisation is used for the lifetime of the compounds, see~~ to be used in the lowermost stratosphere.

In Fig. 9~~. In this figure~~, the zonal maximum of the air pressure where the CH_4 VMR decreases below 1 ppmv (blue dashed) is illustrated along with the zonal minimum of the WMO tropopause pressure (~~see Sect. 2.1) . The air pressure corresponding to 1 ppmv~~ black solid). Additionally, the zonally averaged VMR of CH_4 at the tropopause is shown (red dotted) which ranges from 1.65 (Southern Hemisphere) to 1.7 ppmv (Northern Hemisphere). Due to its relatively long tropospheric lifetime, CH_4 is ~~lower than the tropopause height on the whole latitude range with a minimum difference of about 50 hPa which means that the UTLS region can be investigated using the threshold of in the~~ well-mixed in the troposphere and the CH_4 ~~VMR. Figure 9also includes the~~ VMR does not decrease below 1 ppmv. Above the tropopause, the CH_4 ~~VMR at the tropopause height. As the mainly anthropogenic~~ VMR decreases with height because of higher photolysis rates in the stratosphere.

As can be seen in Fig. 9, the lowest height where the CH_4 ~~emission sources are mostly present in the northern hemisphere, the VMR is higher in the northern than in the southern hemisphere~~VMR decreases below 1 ppmv is clearly above the tropopause so that the OH mechanism is also applied in the lowermost stratosphere.

---

[2] ~~http://www.ecmwf.int/sites/default/files/IFS_CY40R1_Part4.pdf~~

Table 6. Technical description of the simulations used in this study. For the used emission inventories see Table ~~??~~3. Horizontal resolution for the simulations is R2B04 with an advective model time step of ~~460 s~~460 s. Output is given on model layers.

simulation name	time range	output interval (in h)	short description
constL(~~off~~megan-offl)	2004-2015	23	constant lifetime, offline emissions
~~constL(onl~~constL(megan-onl,LAIsun)	2004-2015	23	constant lifetime, biogenic online emissions using LAI$_{sun}$
constL(megan-onl)	2004-2015	23	constant lifetime, biogenic online emissions
OH-chem(~~off~~megan-offl)	2004-2015	23	tracer depletion with OH, offline emissions
OH-chem(~~onl~~megan-onl,LAIsun)	2004-2015	23	tracer depletion with OH, biogenic online emissions using LAI$_{sun}$
OH-chem(megan-onl)	2004-2015	23	tracer depletion with OH, biogenic online emissions

5 ~~The IAGOS-CARIBIC project~~Measurements of acetone

~~In this study, we aim to compare~~

We evaluate our simulations of acetone with observations from a) the KCMP tall tower measurements in Midwestern U.S. for seasonal and interannual variations, and b) the IAGOS-CARIBIC airborne measurements in the UTLS region in a similar way as recently published by Jöckel et al. (2016).

A suite of VOCs including acetone at the KCMP tall tower was measured by a proton transfer reaction mass spectrometer between July 2009 and August 2012 (Hu et al., 2013). The tower (44.6886° N, 93.9728° W, 244 m height above ground) is located at rural area surrounded by croplands. Measurements were carried out 185 m above ground level, providing regional representativeness. The overall measurement uncertainty for acetone averages about 10 %.

In the ongoing project Civil Aircraft for the Regular Investigation of the atmosphere Based on an Instrument Container (IAGOS-CARIBIC) a fully automated laboratory has been integrated into a modified cargo container (Brenninkmeijer et al., 2007). Measuring about 100 trace gases and aerosol parameters, the IAGOS-CARIBIC laboratory is regularly placed on-board a Lufthansa Airbus 340-600 passenger aircraft for up to six consecutive flights per month. The cruising altitude of the aircraft coincides with the UTLS region where measurements have been rare previously. Between 2005 and 2014, the flights took off in Frankfurt whereas the flights nowadays start in Munich in Germany to many intercontinental destinations.

We use the acetone measurements from IAGOS-CARIBIC to compare them with the different innovations in ICON-ART (see Sect. ~~7~~7.3). For our calculations, we use the data of ~~flights~~ the IAGOS-CARIBIC flights with the numbers 110 to 261 and 373 to 528. A statistic of the destinations of these flights can be found in Appendix B.

6 Description of the ICON-ART simulations

We selected ~~four~~ six simulations which are called constL(~~off~~megan-offl), constL(~~onl),~~ megan-onl,LAIsun), constL(megan-onl), OH-chem(~~off)~~megan-offl), OH-chem(megan-onl,LAIsun) and OH-chem(~~onl)~~ megan-onl) hereafter. They are ~~also~~ summarised in Table 6 from a technical point of view.

The simulations are performed with a horizontal resolution of R2B04 (characteristic length of about ~~160 km~~160 km). For output, they are interpolated to a regular 1°x1° longitude-latitude grid. The lowest 46 of total 90 vertical layers are illustrated in Fig. 1. The advective model time step is set to ~~460 s~~460 s. All the simulations include an output interval of ~~23 hours because of the tracers' lifetime in the order of several days to months and therefore a negligible diurnal cycle in the tracer concentrations. Nevertheless, we can consider the temporal variability~~ 23 hours. With this interval, we are able to see the impact of OH ~~with this output interval.~~ on acetone at different times of day without using too many resources. Emissions as described in Table ~~??~~ 3 are added to the tracers' VMR in the lowest model layer~~.~~, see Sect. 3.1.3 for a discussion of this choice.

The meteorological variables such as temperature, pressure and three-dimensional wind as well as sea surface temperature and sea ice cover are initialised with ERA-Interim on 1 January 2004 at 00 UTC in order to cover the IAGOS-CARIBIC time range (2005 – 2015) with a spin-up period of one year for the chemical tracers. CO and CH_4 are initialised based on mean values provided by ~~Monitoring atmospheric composition and climate (MACC) reanalyses~~ MACC reanalysis of January 2004 (Inness et al., 2013). C_3H_8 is initialised based on Pozzer et al. (2010). The initial volume mixing ratio of acetone is set globally to 1 pptv. After initialisation ICON-ART runs freely.

constL(~~off~~megan-offl): The simulation using constant lifetime is the reference simulation for the other simulations. In this simulation, acetone lifetime is set globally to 28 days. This is the mean value of the chemical lifetimes of Jacob et al. (2002), Arnold et al. (2005), Fischer et al. (2012) and Khan et al. (2015). The lifetime of C_3H_8 is set to 14 days. That of CO and CH_4 are parametrised as described in Sect. 4.2 for the whole atmosphere.

constL(megan-onl,LAIsun): Simulation of online biogenic emissions of acetone is performed in this simulation where the offline biogenic acetone emissions in constL(megan-off) are replaced by MEGAN-Online LAI_{sun} (see Sect. 3.2).

constL(~~onl~~megan-onl): Simulation of online biogenic emissions of acetone is performed in this simulation where the offline biogenic acetone emissions in constL(~~off~~megan-off) are replaced by MEGAN-Online LAI.

OH-chem(~~off~~megan-offl): In the simulation including the simplified OH chemistry, the mechanism as illustrated in Sect. 4 is used for depletion of the tracers and therefore replaces the constant lifetime of constL(~~off~~megan-offl).

OH-chem(~~onl~~megan-onl,LAIsun): In this simulation, the ~~biogenic emissions~~ offline biogenic acetone emissions in OH-chem(megan-off) are replaced by MEGAN-Online LAI_{sun}.

OH-chem(megan-onl): Here, the biogenic emissions of acetone are replaced by MEGAN-Online LAI. ~~Apart from that , the configuration is the same as for OH-chem(off) .~~

7 Results

7.1 Comparison of the ICON-ART simulations to ground-based measurements

Near-surface measurements of acetone are rare and no standard output of operational measurements. Data is available for several measurement campaigns such as by Schade and Goldstein (2006) or Fares et al. (2012) but only within one year. As our focus in this study is on the interannual variation of acetone in a climatological sense we here compare our simulations with the tall tower measurements in Minnesota, USA, performed by Hu et al. (2013).

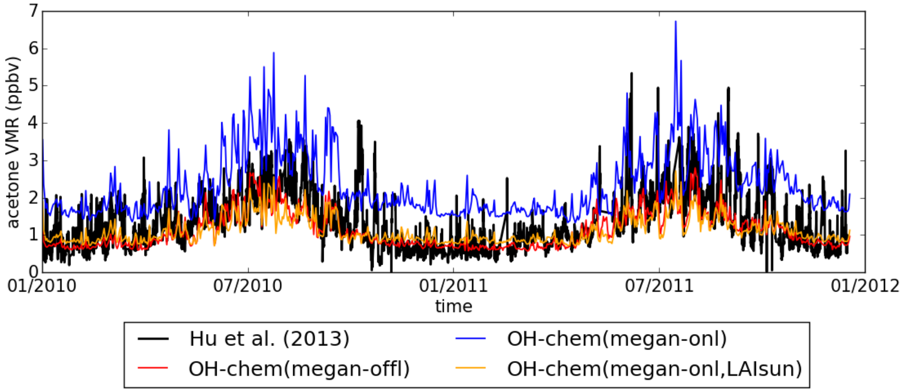

Figure 10. Measured (black) and simulated (red: OH-chem(megan-offl), blue: OH-chem(megan-onl), violet: OH-chem(megan-onl,LAIsun)) acetone VMR interpolated to the observation site in Minnesota (USA), see Hu et al. (2013). The measurement error of 10 % is not included in the figure.

Acetone was measured in a height of 185 m above ground so that the measurements should not be affected too much by local effects such as specific plants at the site. In addition, the measurements include a two years period from 2010 to 2011 and have already been used for a comparison to a global model (Hu et al., 2013).

In Figure 10, we show the results of the three OH-chem simulations together with the full observational time series. For the simulated time series, the horizontal grid point closest to the observation site is chosen and linearly vertically interpolated in geometric height to the measurement height. We cannot expect to simulate the full variability of the time series due to the coarse resolution of the simulation.

The acetone VMR of the OH-chem(megan-onl) simulation (blue line in Fig. 10) is by around factor 2 higher than the observed acetone VMR. Thus, Figure 10 suggests that the emissions of the MEGAN-Online LAI scenario in Fig. 7 are unrealistically high.

In contrast to this, the simulated acetone VMR of OH-chem(megan-offl) and OH-chem(megan-onl,LAIsun) during the summer months (June to August) slightly underestimate the measurements. Altogether, these two time series resemble each other and are in good agreement with the observations. This confirms the previous results related to Figs. 7 and 8 where we have already discussed that the parametrisation of the LAI according to Eq. (7) leads to results comparable with the inventory MEGAN-MACC.

Altogether, we conclude that the emissions module performs well in comparison to the ground-based measurements. The average annual cycle is reflected in all our simulations. The overestimated OH-chem(megan-onl) simulation can be explained by a too large leaf area index (cf. Fig. 8). Especially the OH-chem(megan-offl) and OH-chem(megan-onl,LAIsun) simulations coincide well with the observed time series.

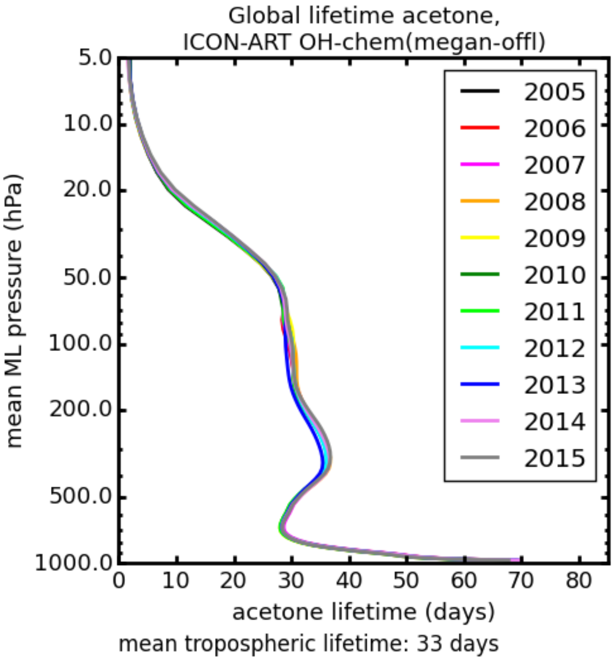

Figure 11. Global lifetime of acetone according to Eq. (13) in the OH-chem simulations averaged for each year. Definition of global lifetime by SPARC (2013) evaluated at each model layer.

7.2 Profile of the acetone lifetime in the OH-chem simulations

In Figure 11, profiles of the annual mean acetone global lifetime according to Eq. (13) during the OH-chem(~~off~~megan-offl) simulation are shown. For pressures higher than $900\,\mathrm{hPa}$, the photolysis rates in Eq. (12) get lower which means that the lifetime is dominated by the depletion with OH, only, leading to lifetimes up to $70\,\mathrm{days}$. In the troposphere and UTLS region, both mechanisms seem to have significant influence on the acetone lifetime. Due to the decrease in water vapour above the tropopause the production of OH by Reaction (R4) decreases. Additionally, the photolysis rates increase in the stratosphere for pressures below $50\,\mathrm{hPa}$ so that the influence of the OH depletion is negligible and the acetone lifetime decreases below one day.

When calculating the mean tropospheric lifetime of acetone according to Eq. (13) in the OH-chem simulations, we derive a value (33 days) comparable to the one (35 days) by Arnold et al. (2005) who also used the definition of SPARC to calculate the acetone lifetime.

7.3 Comparison of the ICON-ART simulations with airborne measurements

Due to the seasonal variability in the biogenic emissions of acetone, its VMR in the mid-latitude UTLS region shows an annual variability with maximum values above $1500\,\mathrm{pptv}$ during summer (Sprung and Zahn, 2010; Elias et al., 2011; Neumaier

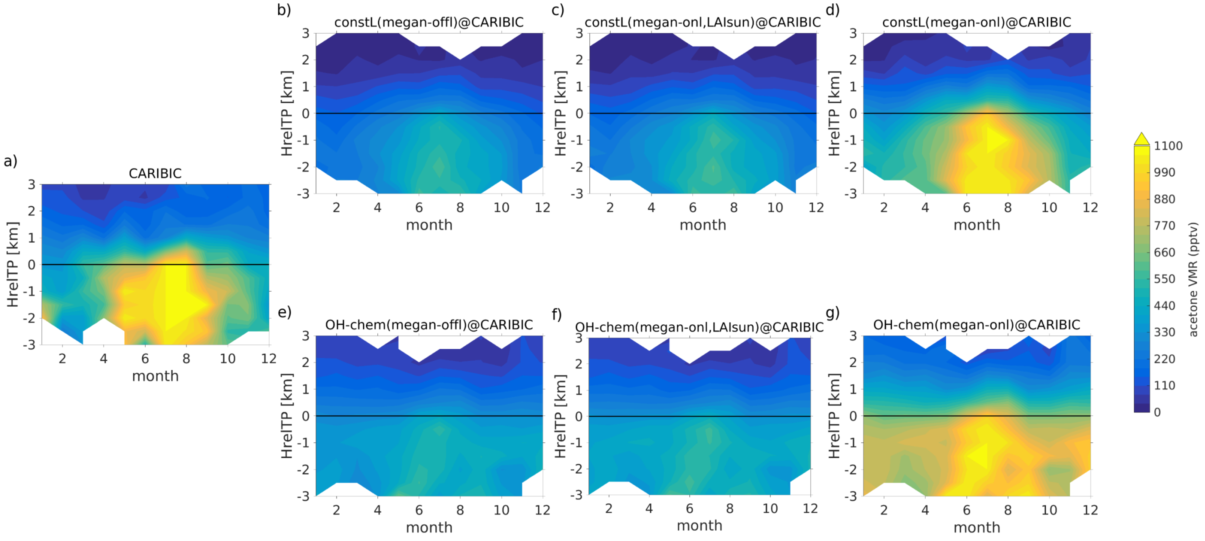

Figure 12. Annual cycles of the acetone VMR of (a) IAGOS-CARIBIC measurements and due to offline MEGAN-MACC (~~middle~~ left column) and MEGAN-Online biogenic emissions with LAI_{sun} (middle column) and LAI (right column). Acetone VMR is shown $\pm 3\,\mathrm{km}$ around the WMO tropopause for constL (first row) and OH-chem simulations (second row). Data is limited to the mid-latitudes between 35 to 75° N and to the pressure range between 180 and $280\,\mathrm{hPa}$. The acetone VMR in the IAGOS-CARIBIC measurements increases up to $1700\,\mathrm{pptv}$ in the maximum.

et al., 2014). This is shown in Fig. 12 where the acetone seasonal cycle $\pm 3\,\mathrm{km}$ around the tropopause is derived from the IAGOS-CARIBIC measurements (panel a) and from the six ICON-ART simulations described in Sect. 6.

In the panels of Fig. 12, the simulated acetone VMR is linearly interpolated in pressure, longitude, latitude and time to the IAGOS-CARIBIC flights (see Eckstein et al., 2016). For calculation of the tropopause height we use the data sets which are most convenient for the measurements and simulations: the underlying temperature profiles for tropopause height in the IAGOS-CARIBIC measurements are derived from ERA-Interim profiles whereas the simulated tropopause height is calculated directly during ~~operation~~ runtime of ICON-ART (see Sect. 2.1). We limit the IAGOS-CARIBIC flights (and correspondingly the model data) to latitudes between 35 and 75° N and exclude descents and ascents of the aeroplane by using data inside the pressure range of 280 and $180\,\mathrm{hPa}$ (similar to Jöckel et al., 2016).

Figure 12 demonstrates that the general annual cycle of acetone can be reproduced with ICON-ART. ~~Maximal~~ Maximum values in the acetone VMR of all ICON-ART simulations occur between June and August where also the measurements maximise. However, differences in the magnitude can be seen: For the simulations driven by offline emissions (~~middle~~ left column) the maximum acetone VMR is underestimated by a factor of 3 with respect to the measurements.

Several reasons could explain this underestimation: (1) ~~The constant acetone lifetime of is too low by a factor of at least 2. This is most unlikely as this value is the mean value of literature values (see Sect. 6) and Fig. 11 suggests a chemical lifetime of acetone in this order of magnitude using the simplified chemistry. (2)~~ We account for chemical production of acetone due to reaction of propane with OH but neglect the contribution of ~~other~~ minor VOCs such as monoterpenes~~so that the acetone VMR could be too low.~~ . The high impact of monoterpenes on acetone calculated by Khan et al. (2015) was recently challenged by Brewer et al. (2017). On the other hand, we neglect the weak uptake of acetone by the oceans and dry deposition which would decrease the acetone VMR slightly (Fischer et al., 2012; Khan et al., 2015). (~~3~~2) The emissions of acetone might be too low. Emission data sets generally are highly uncertain. Sindelarova et al. (2014) estimated an uncertainty in the isoprene emissions of 14 % for the MEGAN-MACC data set. For other VOCs, it could be even higher (e.g. 48.5 % by Williams et al., 2013).

~~Due to the latter reason, we choose the larger online emission with the original leaf area index of ICON (red line in Fig~~As could be expected from Fig. 7, the annual cycles of acetone of constL(megan-onl,LAIsun) and OH-chem(megan-onl,LAIsun) are nearly identical with the respective offline emissions simulations except for slightly higher values in case of the LAIsun simulations. Thus, by parametrising the LAI according to Dai et al. (2004) the online biogenic emissions in ICON-ART are in good agreement with the offline data set MEGAN-MACC. ~~7) for our comparison to the measurements~~

In contrast to this, MEGAN-MACC does not include a parametrised LAI. At least, there is no information given about it in Sindelarova et al. (2014). This is why the resulting acetone VMR of the more than twice larger online emissions using LAI have been suggested to be in agreement with MEGAN-MACC.

The acetone VMR around the tropopause using MEGAN-Online LAI is shown in the rightmost column of Fig. 12. As these emissions are more than twice larger than the offline emissions the acetone VMR is increased in the UTLS region correspondingly. Thus, the differences with reference to observations are reduced but the highest values in the measurements can still not be reached (around 1100 pptv compared to 1700 pptv in the measurements). Apart from the values in the maximum, Fig. 12~~c~~ d using MEGAN-Online LAI combined with constant lifetime of acetone shows the best agreement with the observations in the upper troposphere: the acetone VMR during winter and "near-summer" only differs by 100 pptv or below.

To summarise the last paragraphs, we can reproduce the offline biogenic emissions data set MEGAN-MACC by parametrising the LAI in ICON with Eq. (7). This parametrisation ensures a more realistic treatment of the LAI with respect to the biogenic emissions (Dai et al., 2004). However, the acetone VMR in the UTLS region is underestimated with respect to airborne measurements. The differences to the measurements are reduced if MEGAN-Online LAI is used but the emissions are too high in this case (Fig. 10). Therefore, the question arises if the major sources of acetone are not well represented in the emission inventories used in our simulations and how large the impact of monoterpenes on the chemical production of acetone is in reality (which are not included in the current stage of ICON-ART).

As already mentioned above, the global lifetime of acetone in the OH-chem simulations with a value of 33 days is in the same order of magnitude as in the constL simulations. That is why the maximum values in the acetone VMR in the OH-chem simulations are comparable to the corresponding constL simulations. However, differences occur during winter where the clearly higher acetone lifetime of about 1.5 years in the OH-chem simulations increases the acetone VMR in the UTLS region.

This value is a mid-latitudinal (35 to 75° N) average for the months December to February in 2005 to 2015 in contrast to the global annual average mentioned above.

The comparison of Fig. 12~~e~~ f with the observations demonstrates that the acetone VMR is overestimated by a factor of about 1.5 in the winter months December to February in the upper troposphere. In the lowermost stratosphere and especially above $2\,\mathrm{km}$ of the tropopause height, though, the acetone VMR is improved using the OH chemistry where the observations show higher VMRs than for the case of a constant lifetime (Fig. 12c).

8 Conclusions

We introduce the ~~new interface~~ recently developed module for including emissions from external data sources in ICON-ART. The ~~interface~~ module reads the data interpolated to the ICON grid, interpolates it to the simulation time and adds it to the trace gas volume mixing ratio in ICON-ART. For this, the number of lowest model layers of the emissions $n_{\mathrm{lev,emi}}$ has to be specified where we show a sensitivity test by varying this number. Differences only occur in the height of the emissions itself.

Therefore, the tracer mixing ratio above the emission height $n_{\mathrm{lev,emi}}$ is independent of the choice of $n_{\mathrm{lev,emi}}$. Since the aim of this study is the simulation of acetone in the upper troposphere and lowermost stratosphere (UTLS), we select $n_{\mathrm{lev,emi}} = 1$.

In addition, we demonstrate the online biogenic emission model MEGAN2.1 in the configuration as implemented in ICON-ART ~~.~~ including two parametrisations of the leaf area index (LAI): the unparametrised LAI of ICON (MEGAN-Online LAI scenario) and the LAI parametrised according to Dai et al. (2004) (MEGAN-Online LAI_{sun}).

Emissions using in MEGAN-Online LAI are twice larger than emissions of the offline emission inventory MEGAN-MACC. The emissions of MEGAN-Online LAI_{sun} are comparable to MEGAN-MACC in terms of global means and can therefore be used for investigating the influence of the diurnal cycle on acetone in the atmosphere.

Furthermore, we present a simplified parametrisation to deplete chemical species by reaction with OH. The OH concentration is calculated as steady state: it is produced by photolysis of ozone and reaction of the produced $\mathrm{O(^1D)}$ with water vapour. It is depleted by reactions with $\mathrm{CH_4}$ and CO.

With these new features, it is now possible to simulate volatile compounds (VOCs) with ICON-ART reliably. We illustrate this with acetone as one member of the VOCs.

~~We investigate the influence of the different features by comparing them to airborne measurements of the IAGOS-CARIBIC project in the upper troposphere and lowermost stratosphere (UTLS). We test two parametrisations of the leaf area index (LAI)~~ Compared to ground-based measurements of Hu et al. (2013), our simulations generally show a comparable seasonal cycle. Due to the higher emissions the acetone volume mixing ratio is overestimated with MEGAN-Online LAI. In contrast to this, the simulations with offline emissions and online biogenic emissions of MEGAN-Online LAI_{sun} are in good agreement with the observations with slight underestimation during summer. This demonstrates that the correct treatment of the LAI in MEGAN2.1 ~~for October 2007: emissionsusing the LAI of ICON are twice as high than the emissions of the offline emission inventory MEGAN-MACC. The emissions due to the parametrised LAI according to Dai et al. (2004) are comparable to MEGAN-MACC in terms of global means and can therefore be used for investigating the influence of~~ is crucial to get realistic results for online biogenic emissions. Further investigation of the ~~diurnal cycle on acetone in the atmosphere. In order to account for the uncertainty in the emission inventories we show results of~~ representation of the emissions in MEGAN2.1 ~~using the LAI of ICON.~~ will follow in the future.

We also investigate the influence of the different features by comparing them to airborne measurements of the IAGOS-CARIBIC project in the UTLS region. With offline emissions and with online emissions of MEGAN-Online LAI_{sun} the acetone VMR in the UTLS region is underestimated by factor of 3. Correspondingly, it is increased by ~~replacing offline with online biogenic~~ using the unparametrised LAI of ICON for online emissions. The simplified OH chemistry leads to a higher acetone lifetime especially during winter which results in an overestimation of the acetone VMR within December and February by a factor of about 1.5. On the other hand, the acetone VMR in the lowermost stratosphere is improved by using the OH depletion mechanism.

Altogether, we show that the general acetone annual cycle is well represented in the model compared to the ground-based observations as well as to airborne IAGOS-CARIBIC measurements with a maximum during summer and a minimum during winter. Considering the acetone distribution in the lowest model layer we demonstrate that the presented emission ~~interface~~ module performs well. In addition, the calculated tropospheric acetone lifetime of 33 days is in good agreement with Arnold et al. (2005) who used the same method to derive it. This value suggests that the new parametrisation of tracer depletion with OH is a good estimate of the OH concentration in the troposphere.

Code availability

~~The code of~~ Currently the legal departments of Max Planck Institute for Meteorology (MPI-M) and DWD are finalising the ICON license. If you want to obtain ICON-ART ~~version 2.0 can be downloaded via the following link:~~ you will first need to sign an institutional ICON license which you will get by sending a request to icon@dwd.de. In a second step you will get the ART license by contacting Bernhard Vogel (bernhard.vogel@kit.edu).

~~link~~

Appendix A: Predictor-corrector method

In this section, we explain the discretisation method for tracer concentration changes. We here refer to “concentration” as an abbreviation of number concentration (unit molecules per volume unit). Concentrations of tracers are determined by solving the following differential equation:

$$\frac{\mathrm{d}c_i}{\mathrm{d}t}\frac{\partial c_i(x,t)}{\partial t} = P_i(x,t) - c_i(x,t)\,L_i(x,t) \tag{A1}$$

with c_i, P_i and L_i as concentration, chemical production and loss rate of tracer i. Concentration, chemical production and loss rate depend on location x and time t. In ICON-ART version 1.0, this equation was discretised with the explicit Euler method (Rieger et al., 2015), omitting the index i ~~(Rieger et al., 2015)~~and the location dependence:

$$c_{\underline{n+1}\,t+\Delta t}^{(e)} = c_{\underline{n}\,t}^{(e)} + \left(P_{\underline{n}\,t} - c_{\underline{n}\,t}^{(e)}\,L_{\underline{n}\,t}\right)\underline{\cdot}\,\Delta t \tag{A2}$$

~~In this equation, the index n stands for the nth model time step.~~ Too low values of the tracer's lifetime can lead to solutions that do not converge to the differential equation (A1). Since fully implicit methods generally are expensive in computation resources, ~~Seinfeld and Pandis (2012)~~ Seinfeld and Pandis (2012, pp. 1125–1126) suggest a two-step predictor-corrector discretisation method for solving Eq. (A1) which is discussed in this section. This method reasonably closes the gap between the low computation effort for explicit discretisation methods on the one hand and the accuracy and stability of implicit methods on the other hand.

Please note that the lifetime τ_t in this section is the reciprocal value of the loss rate~~(compared~~ : $\tau_t = 1/L_t$ (in contrast to the definition of SPARC used in the other sections).

Generally, Equation (A1) can be discretised implicitly as follows ~~(Seinfeld and Pandis, 2012)~~(Seinfeld and Pandis, 2012, pp. 1125–1126

$$c_{\underline{n+1}\,t+\Delta t}^{(\mathrm{ipc})} = \underline{\frac{c_n\cdot(\tau_{n+1}+\tau_n-\Delta t)+0.5\,\Delta t\,(P_{n+1}+P_n)\,(\tau_{n+1}+\tau_n)}{\tau_{n+1}+\tau_n+\Delta t}}\;\frac{c_t^{(\mathrm{ipc})}\,(\tau_{t+\Delta t}+\tau_t-\Delta t)+0.5\,\Delta t\,(P_{t+\Delta t}+P_t)\,(\tau_{t+\Delta t}+\tau_t)}{\tau_{t+\Delta t}+\tau_t+\Delta t} \tag{A3}$$

Lifetimes and productions of the next time step, denoted by index ~~$n+1$~~$t+\Delta t$, are not defined at time step ~~n~~t. That is why they have to be approximated before Eq. (A3) can be evaluated.

In a first step, called the predictor step, the new concentrations c_* are approximated by assuming constant lifetime and production (~~$\tau_{n+1}=\tau_n$ and $P_{n+1}=P_n$~~$\tau_{t+\Delta t}=\tau_t$ and $P_{t+\Delta t}=P_t$):

$$c_* = \underline{\frac{c_n\cdot(2\,\tau_n-\Delta t)+2\Delta t\,\tau_n\,P_n}{2\,\tau_n+\Delta t}}\;\frac{c_t\,(2\,\tau_t-\Delta t)+2\Delta t\,\tau_t\,P_t}{2\,\tau_t+\Delta t} \tag{A4}$$

In this study, these concentrations are calculated for CH_4, CO, propane and acetone. This is an inaccurate estimation of the concentrations of the next time step since lifetime and production both can vary within one time step ~~(Seinfeld and Pandis, 2012)~~(Seinfeld a
For improving accuracy, the lifetimes and productions of the next time step are approximated with the c_* of Eq. (A4). For that purpose, c_* is used for calculating a new OH number concentration, $[\mathrm{OH}]_*$, as described in Sect. 4.1. In turn, with $[\mathrm{OH}]_*$, the lifetimes and chemical productions of the next time step can be approximated, denoted as τ_* and P_*, respectively.

Then, the so-called corrector step can be executed in order to get the tracer concentrations of the next time step by replacing ~~τ_{n+1} and P_{n+1}~~ $\tau_{t+\Delta t}$ and $P_{t+\Delta t}$ in Eq. (A3) by their approximations τ_* and P_*, respectively:

$$c_{\underline{n+1}\,t+\Delta t}^{(\mathrm{pc})} = \underline{\frac{c_n \cdot (\tau_* + \tau_n - \Delta t) + 0.5\,\Delta t\,(P_* + P_n)\,(\tau_* + \tau_n)}{\tau_* + \tau_n + \Delta t}}\,\frac{c_t^{(\mathrm{pc})}\,(\tau_* + \tau_t - \Delta t) + 0.5\,\Delta t\,(P_* + P_t)\,(\tau_* + \tau_t)}{\tau_* + \tau_t + \Delta t} \tag{A5}$$

If ~~the expression $\tau_* + \tau_n$ gets lower than~~ Δt becomes larger than the expression $\tau_* + \tau_t$, this method also ~~gets instable.~~ can get instable.

To illustrate this, consider the following example by assuming the chemical production P in Eq. (A5) to be zero, i.e.: $P_* = P_n = 0$ and additionally $\tau_* + \tau_n - \Delta t < 0$. In this case, the concentration of the next time step $c_{t+\Delta t}^{(\mathrm{pc})}$ becomes negative which obviously shows that the numerical solution does not converge the physical solution of the differential equation of Eq. (A1).

That is why we use the fully implicit Euler method assuming constant lifetime and chemical production if the lifetime gets lower than Δt:

$$c_{\underline{n+1}\,t+\Delta t}^{(\mathrm{i})} = P_{\underline{n}\,t}\,\tau_{\underline{n}\,t} + \left(c_{\underline{n}\,t}^{(\mathrm{i})} - P_{\underline{n}\,t}\,\tau_{\underline{n}\,t}\right) \underline{\cdot} \exp\left(-\underline{\frac{\Delta t}{\tau_n}}\,\frac{\Delta t}{\tau_t}\right), \quad \tau_{\underline{n}\,t} < \Delta t \tag{A6}$$

Appendix B: Statistic of the used CARIBIC flights

Here, we show the destinations of all the CARIBIC flights used in the results. The statistic can be found in Table 7. For this, we counted the return flights as one flight and did not count stopovers of the aircraft as separate flights.

Acknowledgements. ~~We~~ We thank Christoph A. Keller (NASA) for giving us details about the treatment of emissions within GEOS-Chem. We acknowledge ECCAD for archiving and distributing the data. This study was performed on the computational resource ForHLR II funded by the Ministry of Science, Research and the Arts Baden-Württemberg and DFG ("Deutsche Forschungsgemeinschaft").

Table 7. Frequency of occurrence of the destinations in the CARIBIC flights used for the climatologies in Sect. 7. The total number of different flights is 113.

destination	number of flights
Manila (Philippines)[a]	21
Chennai (India)	18
Caracas (Venezuela)	11
Kuala Lumpur (Malaysia)[b]	8
Sao Paulo (Brazil)	8
Vancouver (Canada)	8
Santiago (Chile)[c]	7
Seoul (South Korea)	7
San Francisco (USA)	7
Los Angeles (USA)	4
Tokyo (Japan)	3
Toronto (Canada)	2
Denver (USA)	2
Houston (USA)	1
Bogota (Columbia)	1
Rio de Janeiro (Brazil)	1
Beijing (China)	1
Cape Town (South Africa)	1
Mexico City (Mexico)	1
Hong Kong (Hong Kong)	1

stopover in [a] Guangzhou, [b] Bangkok and [c] Sao Paulo

References

Arnold, S., Chipperfield, M., and Blitz, M.: A three-dimensional model study of the effect of new temperature-dependent quantum yields for acetone photolysis, J. Geophys. Res.: Atmosphere, 110, doi:10.1029/2005JD005998, 2005.

Atkinson, R. and Arey, J.: Atmospheric Degradation of Volatile Organic Compounds, Chemical Reviews, 103, 4605–4638, doi:10.1021/cr0206420, 2003.

Atkinson, R., Baulch, D. L., Cox, R. A., Crowley, J. N., Hampson, R. F., Hynes, R. G., Jenkin, M. E., Rossi, M. J., Troe, J., and IUPAC Subcommittee: Evaluated kinetic and photochemical data for atmospheric chemistry: Volume II - gas phase reactions of organic species, Atmos. Chem. Phys., 6, 3625–4055, doi:10.5194/acp-6-3625-2006, 2006.

Baldauf, M., Seifert, A., Förstner, J., Majewski, D., Raschendorfer, M., and Reinhardt, T.: Operational Convective-Scale Numerical Weather Prediction with the COSMO Model: Description and Sensitivities, Mon. Weather Rev., 139, 3887–3905, doi:10.1175/MWR-D-10-05013.1, 2011.

Bey, I., Jacob, D. J., Yantosca, R. M., Logan, J. A., Field, B. D., Fiore, A. M., Li, Q., Liu, H. Y., Mickley, L. J., and Schultz, M. G.: Global modeling of tropospheric chemistry with assimilated meteorology: Model description and evaluation, J. Geophys. Res.: Atmospheres, 106, 23 073–23 095, doi:10.1029/2001JD000807, 2001.

Blake, N. and Blake, D.: Tropospheric Chemistry and Composition: VOCs: Overview in Encyclopedia of Atmospheric Sciences Edited by J. R. Holton, J. A. Pyle, and J. A. Curry, Academic Press, doi:10.1006/rwas.2002.0422, 2002.

Boucher, O., Haigh, J., Hauglustaine, D., Haywood, J., Myhre, G., Nakajima, T., Shi, G., and Solomon, S., eds.: *Radiative Forcing of Climate Change. In:* Climate Change 2001: The Scientific Basis. Contribution of Working Group I to the Third Assessment Report of the Intergovernmental Panel on Climate Change, Cambridge University Press, Cambridge, United Kingdom and New York, NY, USA, 2001.

Brasseur, G. and Solomon, S.: Aeronomy of the Middle Atmosphere, Atmospheric sciences library, D. Reidel Publishing Company, Dordrecht, 2nd edn., 1995.

Brenninkmeijer, C., Crutzen, P., Boumard, F., Dauer, T., Dix, B., Ebinghaus, R., Filippi, D., Fischer, H., Franke, H., Frieß, U., et al.: Civil Aircraft for the regular investigation of the atmosphere based on an instrumented container: The new CARIBIC system, Atmos. Chem. Phys., 7, 4953–4976, doi:10.5194/acp-7-4953-2007, 2007.

Brewer, J. F., Bishop, M., Kelp, M., Keller, C., Ravishankara, A. R., and Fischer, E. V.: A sensitivity analysis of key natural factors in the modeled global acetone budget, J. Geophys. Res.: Atmospheres, doi:10.1002/2016JD025935, 2016JD025935, 2017.

Dai, Y., Dickinson, R., and Wang, Y.: A Two-Big-Leaf Model for Canopy Temperature, Photosynthesis, and Stomatal Conductance, J. Clim., 17, 2281–2299, doi:10.1175/1520-0442(2004)017<2281:ATMFCT>2.0.CO;2, 2004.

Diehl, T., Heil, A., Chin, M., Pan, X., Streets, D., Schultz, M., and Kinne, S.: Anthropogenic, biomass burning, and volcanic emissions of black carbon, organic carbon, and SO_2 from 1980 to 2010 for hindcast model experiments, Atmos. Chem. Phys. Discuss., 12, 24 895–24 954, doi:10.5194/acpd-12-24895-2012, 2012.

Doms, G. and Schättler, U.: A description of the nonhydrostatic regional model LM. Part II: Physical parameterization, Tech. rep., Deutscher Wetterdienst, Offenbach, 2004.

Dunlea, E. J. and Ravishankara, A. R.: Measurement of the rate coefficient for the reaction of $O(^1D)$ with H_2O and re-evaluation of the atmospheric OH production rate, Phys. Chem. Chem. Phys., 6, 3333–3340, doi:10.1039/B402483D, 2004.

Eckstein, J., Ruhnke, R., Zahn, A., Neumaier, M., Kirner, O., and Braesicke, P.: An assessment of the climatological representativeness of IAGOS-CARIBIC trace gas measurements using EMAC model simulations, Atmos. Chem. Phys. Discuss., 2016, 1–25, doi:10.5194/acp-2016-179, accepted for publication in ACP, 2016.

Elbern, H., Schwinger, J., and Botchorishvili, R.: Chemical state estimation for the middle atmosphere by four-dimensional variational data assimilation: System configuration, J. Geophys. Res.: Atmospheres, 115, doi:10.1029/2009JD011953, d06302, 2010.

Elias, T., Szopa, S., Zahn, A., Schuck, T., Brenninkmeijer, C., Sprung, D., and Slemr, F.: Acetone variability in the upper troposphere: analysis of CARIBIC observations and LMDz-INCA chemistry-climate model simulations, Atmos. Chem. Phys., 11, 8053–8074, doi:10.5194/acp-11-8053-2011, 2011.

Elshorbany, Y. F., Duncan, B. N., Strode, S. A., Wang, J. S., and Kouatchou, J.: The description and validation of the computationally Efficient CH4-CO-OH (ECCOHv1.01) chemistry module for 3-D model applications, Geosci. Model Dev., 9, 799–822, doi:10.5194/gmd-9-799-2016, 2016.

Fares, S., Park, J.-H., Gentner, D. R., Weber, R., Ormeño, E., Karlik, J., and Goldstein, A. H.: Seasonal cycles of biogenic volatile organic compound fluxes and concentrations in a California citrus orchard, Atmos. Chem. Phys., 12, 9865–9880, doi:10.5194/acp-12-9865-2012, 2012.

Field, C. B., Randerson, J. T., and Malmström, C. M.: Global net primary production: Combining ecology and remote sensing, Remote Sens. Environ., 51, 74 – 88, doi:10.1016/0034-4257(94)00066-V, 1995.

Fischer, E., Jacob, D. J., Millet, D., Yantosca, R. M., and Mao, J.: The role of the ocean in the global atmospheric budget of acetone, Geophys. Res. Lett., 39, doi:10.1029/2011GL050086, L01807, 2012.

Folkins, I. and Chatfield, R.: Impact of acetone on ozone production and OH in the upper troposphere at high $\mathrm{NO_x}$, J. Geophys. Res.: Atmospheres, 105, 11 585–11 599, doi:10.1029/2000JD900067, 2000.

Gent, P. R., Danabasoglu, G., Donner, L. J., Holland, M. M., Hunke, E. C., Jayne, S. R., Lawrence, D. M., Neale, R. B., Rasch, P. J., Vertenstein, M., Worley, P. H., Yang, Z.-L., and Zhang, M.: The Community Climate System Model Version 4, J. Clim., 24, 4973–4991, doi:10.1175/2011JCLI4083.1, 2011.

Goto, D., Dai, T., Satoh, M., Tomita, H., Uchida, J., Misawa, S., Inoue, T., Tsuruta, H., Ueda, K., Ng, C. F. S., Takami, A., Sugimoto, N., Shimizu, A., Ohara, T., and Nakajima, T.: Application of a global nonhydrostatic model with a stretched-grid system to regional aerosol simulations around Japan, Geosci. Model Dev., 8, 235–259, doi:10.5194/gmd-8-235-2015, 2015.

Granier, C., Bessagnet, B., Bond, T., D'Angiola, A., Denier van der Gon, H., Frost, G., Heil, A., Kaiser, J., Kinne, S., Klimont, Z., Kloster, S., Lamarque, J.-F., Liousse, C., Masui, T., Meleux, F., Mieville, A., Ohara, T., Raut, J.-C., Riahi, K., Schultz, M., Smith, S., Thompson, A., van Aardenne, J., van der Werf, G., and van Vuuren, D.: Evolution of anthropogenic and biomass burning emissions of air pollutants at global and regional scales during the 1980-2010 period, Clim. Change, 109, 163–190, doi:10.1007/s10584-011-0154-1, 2011.

Grell, G. A., Peckham, S. E., Schmitz, R., McKeen, S. A., Frost, G., Skamarock, W. C., and Eder, B.: Fully coupled online chemistry within the WRF model, Atmos. Environ., 39, 6957–6975, doi:10.1016/j.atmosenv.2005.04.027, 2005.

Guenther, A., Jiang, X., Heald, C., Sakulyanontvittaya, T., Duhl, T., Emmons, L., and Wang, X.: The Model of Emissions of Gases and Aerosols from Nature version 2.1 (MEGAN2.1): an extended and updated framework for modeling biogenic emissions, Geosci. Model Dev., 5, 1471–1492, doi:10.5194/gmd-5-1471-2012, 2012.

Heikes, B. G., Chang, W., Pilson, M. E. Q., Swift, E., Singh, H. B., Guenther, A., Jacob, D. J., Field, B. D., Fall, R., Riemer, D., and Brand, L.: Atmospheric methanol budget and ocean implication, Global Biogeochem. Cycles, 16, 80–1–80–13, doi:10.1029/2002GB001895, 1133, 2002.

Hollingsworth, A., Engelen, R., Benedetti, A., Dethof, A., Flemming, J., Kaiser, J., Morcrette, J., Simmons, J., Textor, C., Boucher, O., Chevallier, F., Rayner, P., Elbern, H., Eskes, H., Granier, C., Peuch, V., Rouil, L., and Schultz, M.: Toward a monitoring and forecasting system for atmospheric composition: the GEMS project, Bull. Amer. Meteor. Soc., 89, 1147–1164, doi:10.1175/2008BAMS2355.1, 2008.

Hu, L., Millet, D. B., Kim, S. Y., Wells, K. C., Griffis, T. J., Fischer, E. V., Helmig, D., Hueber, J., and Curtis, A. J.: North American acetone sources determined from tall tower measurements and inverse modeling, Atmos. Chem. Phys., 13, 3379–3392, doi:10.5194/acp-13-3379-2013, 2013.

Inness, A., Baier, F., Benedetti, A., Bouarar, I., Chabrillat, S., Clark, H., Clerbaux, C., Coheur, P., Engelen, R. J., Errera, Q., Flemming, J., George, M., Granier, C., Hadji-Lazaro, J., Huijnen, V., Hurtmans, D., Jones, L., Kaiser, J. W., Kapsomenakis, J., Lefever, K., Leitão, J., Razinger, M., Richter, A., Schultz, M. G., Simmons, A. J., Suttie, M., Stein, O., Thépaut, J.-N., Thouret, V., Vrekoussis, M., Zerefos, C., and the MACC team: The MACC reanalysis: an 8 yr data set of atmospheric composition, Atmos. Chem. Phys., 13, 4073–4109, doi:10.5194/acp-13-4073-2013, 2013.

Jacob, D. J.: Introduction to atmospheric chemistry, Princeton Univ. Press, Princeton, NJ, 1st edn., 1999.

Jacob, D. J., Field, B. D., Jin, E. M., Bey, I., Li, Q., Logan, J. A., Yantosca, R. M., and Singh, H. B.: Atmospheric budget of acetone, J. Geophys. Res.: Atmosphere, 107, ACH 5–1–ACH 5–17, doi:10.1029/2001JD000694, 2002.

Jaeglé, L., Jacob, D. J., Brune, W., Tan, D., Faloona, I., Weinheimer, A., Ridley, B., Campos, T., and Sachse, G.: Sources of HOx and production of ozone in the upper troposphere over the United States, Geophys. Res. Lett., 25, 1709–1712, doi:10.1029/98GL00041, 1998.

Janssens-Maenhout, G., Petrescu, A. M., Muntean, M., and Blujdea, V.: Verifying Greenhouse Gas Emissions: Methods to Support International Climate Agreements, Greenhouse Gas Measurement and Management, 1, 132–133, doi:10.1080/20430779.2011.579358, 2011.

Janssens-Maenhout, G., Diego, V., and Marilena Muntean, G.: Global emission inventories in the Emission Database for Global Atmospheric Research (EDGAR)–Manual (I), Gridding: EDGAR emissions distribution on global gridmaps, Publications Office of the European Union, Luxembourg, 2013.

Jöckel, P., Sander, R., Kerkweg, A., Tost, H., and Lelieveld, J.: Technical Note: The Modular Earth Submodel System (MESSy) - a new approach towards Earth System Modeling, Atmos. Chem. Phys., 5, 433–444, doi:10.5194/acp-5-433-2005, 2005.

Jöckel, P., Tost, H., Pozzer, A., Brühl, C., Buchholz, J., Ganzeveld, L., Hoor, P., Kerkweg, A., Lawrence, M.-G., Sander, R., Steil, B., Stiller, G., Tanarhte, M., Taraborrelli, D., van Aardenne, J., and Lelieveld, J.: The atmospheric chemistry general circulation model ECHAM5/MESSy1: consistent simulation of ozone from the surface to the mesosphere, Atmos. Chem. Phys., 6, 5067–5104, doi:10.5194/acp-6-5067-2006, 2006.

Jöckel, P., Tost, H., Pozzer, A., Kunze, M., Kirner, O., Brenninkmeijer, C. A. M., Brinkop, S., Cai, D. S., Dyroff, C., Eckstein, J., Frank, F., Garny, H., Gottschaldt, K.-D., Graf, P., Grewe, V., Kerkweg, A., Kern, B., Matthes, S., Mertens, M., Meul, S., Neumaier, M., Nützel, M., Oberländer-Hayn, S., Ruhnke, R., Runde, T., Sander, R., Scharffe, D., and Zahn, A.: Earth System Chemistry integrated Modelling (ESCiMo) with the Modular Earth Submodel System (MESSy) version 2.51, Geosci. Model Dev., 9, 1153–1200, doi:10.5194/gmd-9-1153-2016, 2016.

Keller, C. A., Long, M. S., Yantosca, R. M., Da Silva, A. M., Pawson, S., and Jacob, D. J.: HEMCO v1.0: a versatile, ESMF-compliant component for calculating emissions in atmospheric models, Geosci. Model Dev., 7, 1409–1417, doi:10.5194/gmd-7-1409-2014, 2014.

Kerkweg, A., Sander, R., Tost, H., and Jöckel, P.: Technical note: Implementation of prescribed (OFFLEM), calculated (ONLEM), and pseudo-emissions (TNUDGE) of chemical species in the Modular Earth Submodel System (MESSy), Atmos. Chem. Phys., 6, 3603–3609, doi:10.5194/acp-6-3603-2006, 2006.

Khan, M., Cooke, M., Utembe, S., Archibald, A., Maxwell, P., Morris, W., Xiao, P., Derwent, R., Jenkin, M., Percival, C., Walsh, R., Young, T., Simmonds, P., Nickless, G., O'Doherty, S., and Shallcross, D.: A study of global atmospheric budget and distribution of acetone using global atmospheric model STOCHEM-CRI, Atmos. Environ., 112, 269 – 277, doi:10.1016/j.atmosenv.2015.04.056, 2015.

Kouker, W., Offermann, D., Küll, V., Reddmann, T., Ruhnke, R., and Franzen, A.: Streamers observed by the CRISTA experiment and simulated in the KASIMA model, J. Geophys. Res.: Atmospheres, 104, 16 405–16 418, doi:10.1029/1999JD900177, 1999.

Lamarque, J.-F., Bond, T. C., Eyring, V., Granier, C., Heil, A., Klimont, Z., Lee, D., Liousse, C., Mieville, A., Owen, B., Schultz, M. G., Shindell, D., Smith, S. J., Stehfest, E., Van Aardenne, J., Cooper, O. R., Kainuma, M., Mahowald, N., McConnell, J. R., Naik, V., Riahi, K., and van Vuuren, D. P.: Historical (1850-2000) gridded anthropogenic and biomass burning emissions of reactive gases and aerosols: methodology and application, Atmos. Chem. Phys., 10, 7017–7039, doi:10.5194/acp-10-7017-2010, 2010.

Lamarque, J.-F., Emmons, L. K., Hess, P. G., Kinnison, D. E., Tilmes, S., Vitt, F., Heald, C. L., Holland, E. A., Lauritzen, P. H., Neu, J., Orlando, J. J., Rasch, P. J., and Tyndall, G. K.: CAM-chem: description and evaluation of interactive atmospheric chemistry in the Community Earth System Model, Geosci. Model Dev., 5, 369–411, doi:10.5194/gmd-5-369-2012, 2012.

Lauritzen, P. H., Erath, C., and Mittal, R.: On simplifying 'incremental remap' - based transport schemes, J. Comp. Phys., 230, 7957–7963, doi:10.1016/j.jcp.2011.06.030, 2011.

Lawrence, P. J. and Chase, T. N.: Representing a new MODIS consistent land surface in the Community Land Model (CLM 3.0), J. Geophys. Res.: Biogeosciences, 112, doi:10.1029/2006JG000168, g01023, 2007.

Leuenberger, D., Koller, M., Fuhrer, O., and Schär, C.: A generalization of the SLEVE vertical coordinate, Mon. Weather Rev., 138, 3683–3689, doi:10.1175/2010MWR3307.1, 2010.

McKeen, S. A., Hsie, E.-Y., Trainer, M., Tallamraju, R., and Liu, S. C.: A regional model study of the ozone budget in the eastern United States, J, Geophys. Res.: Atmospheres, 96, 10 809–10 845, doi:10.1029/91JD00052, 1991.

Miura, H.: An Upwind-Biased Conservative Advection Scheme for Spherical Hexagonal-Pentagonal Grids, Mon. Wea. Rev., 135, 4038–4044, doi:10.1175/2007MWR2101.1, 2007.

Neale, R. B., Richter, J., Park, S., Lauritzen, P. H., Vavrus, S. J., Rasch, P. J., and Zhang, M.: The Mean Climate of the Community Atmosphere Model (CAM4) in Forced SST and Fully Coupled Experiments, J. Clim., 26, 5150–5168, doi:10.1175/JCLI-D-12-00236.1, 2013.

Neumaier, M., Ruhnke, R., Kirner, O., Ziereis, H., Stratmann, G., Brenninkmeijer, C., and Zahn, A.: Impact of acetone (photo) oxidation on HOx production in the UT/LMS based on CARIBIC passenger aircraft observations and EMAC simulations, Geophys. Res. Lett., 41, 3289–3297, doi:10.1002/2014GL059480, 2014.

Niwa, Y., Tomita, H., Satoh, M., and Imasu, R.: A Three-Dimensional Icosahedral Grid Advection Scheme Preserving Monotonicity and Consistency with Continuity for Atmospheric Tracer Transport, J. Meteorolog. Soc. Jpn. Ser. II, 89, 255–268, doi:10.2151/jmsj.2011-306, 2011.

Olivier, J. and Janssens-Maenhout, G.: CO_2 emissions from fossil fuel combustion: 2015 edition: Part III: Total greenhouse gas emissions, Tech. rep., jRC99764, 2015.

Potter, C. S., Randerson, J. T., Field, C. B., Matson, P. A., Vitousek, P. M., Mooney, H. A., and Klooster, S. A.: Terrestrial ecosystem production: a process model based on global satellite and surface data, Global Biogeochem. Cycles, 7, 811–841, doi:10.1029/93GB02725, 1993.

Pozzer, A., Pollmann, J., Taraborrelli, D., Jöckel, P., Helmig, D., Tans, P., Hueber, J., and Lelieveld, J.: Observed and simulated global distribution and budget of atmospheric C_2-C_5 alkanes, Atmos. Chem. Phys., 10, 4403–4422, doi:10.5194/acp-10-4403-2010, 2010.

Prather, M. J.: Photolysis rates in correlated overlapping cloud fields: Cloud-J 7.3c, Geosci. Model Dev., 8, 2587–2595, doi:10.5194/gmd-8-2587-2015, 2015.

Prill, F.: DWD ICON Tools Documentation (software revision 764), Deutscher Wetterdienst, Offenbach, 2016.

Randerson, J. T., Thompson, M. V., Malmström, C. M., Field, C. B., and Fung, I. Y.: Substrate limitations for heterotrophs: Implications for models that estimate the seasonal cycle of atmospheric CO_2, Global Biogeochem. Cycles, 10, 585–602, doi:10.1029/96GB01981, 1996.

Rieger, D., Bangert, M., Bischoff-Gauss, I., Förstner, J., Lundgren, K., Reinert, D., Schröter, J., Vogel, H., Zängl, G., Ruhnke, R., and Vogel, B.: ICON-ART 1.0 - a new online-coupled model system from the global to regional scale, Geosci. Model Dev., 8, 1659–1676, doi:10.5194/gmd-8-1659-2015, 2015.

Rosado-Reyes, C. M. and Francisco, J. S.: Atmospheric oxidation pathways of propane and its by-products: Acetone, acetaldehyde, and propionaldehyde, J. Geophys. Res.: Atmosphere, 112, doi:10.1029/2006JD007566, D14310, 2007.

Ruhnke, R., Kouker, W., and Reddmann, T.: The influence of the $OH + NO_2 + M$ reaction on the NO_y, partitioning in the late Arctic winter 1992/1993 as studied with KASIMA, J. Geophys. Res.: Atmospheres, 104, 3755–3772, doi:10.1029/1998JD100062, 1999.

Sander, S., Abbatt, J., Barker, J., Burkholder, J., Friedl, R., Golden, D., Huie, R., Kolb, C., Kurylo, M., Moortgat, K., Orkin, V., and Wine, P.: Chemical Kinetics and Photochemical Data for Use in Atmospheric Studies, Evaluation No. 17, JPL Publication 10-6, 2011.

Schade, G. W. and Goldstein, A. H.: Seasonal measurements of acetone and methanol: Abundances and implications for atmospheric budgets, Global Biogeochem. Cycles, 20, doi:10.1029/2005GB002566, gB1011, 2006.

Seifert, A.: A short introduction to microphysics in the NWP ICON model, Tech. rep., Deutscher Wetterdienst, Offenbach, 2010.

Seinfeld, J. H. and Pandis, S. N.: Atmospheric Chemistry and Physics: From Air Pollution to Climate Change, John Wiley & Sons, 2nd edn., 2012.

Shao, M. and Wildt, J.: Quantification of acetone emission from pine plants, Sci. China, Ser. B Chem., 45, 532–540, doi:10.1360/02yb9070, 2002.

Simmons, A. J., Burridge, D. M., Jarraud, M., Girard, C., and Wergen, W.: The ECMWF medium-range prediction models development of the numerical formulations and the impact of increased resolution, Meteorol. Atmos. Phys., 40, 28–60, doi:10.1007/BF01027467, Documentation:http://www.ecmwf.int/sites/default/files/elibrary/2014/9204-part-iv-physical-processes.pdf, 1989.

Sindelarova, K., Granier, C., Bouarar, I., Guenther, A., Tilmes, S., Stavrakou, T., Müller, J.-F., Kuhn, U., Stefani, P., and Knorr, W.: Global data set of biogenic VOC emissions calculated by the MEGAN model over the last 30 years, Atmos. Chem. Phys., 14, 9317–9341, doi:10.5194/acp-14-9317-2014, 2014.

Singh, H. B., Kanakidou, M., Crutzen, P., and Jacob, D.: High concentrations and photochemical fate of oxygenated hydrocarbons in the global troposphere, Nature, 378, 50–54, doi:10.1038/378050a0, 1995.

SPARC: SPARC Report on Lifetimes of Stratospheric Ozone-Depleting Substances, Their Replacements, and Related Species, Tech. rep., SPARC, 2013.

Sprung, D. and Zahn, A.: Acetone in the upper troposphere/lowermost stratosphere measured by the CARIBIC passenger aircraft: Distribution, seasonal cycle, and variability, J. Geophys. Res.: Atmosphere, 115, doi:10.1029/2009JD012099, 2010.

Stassen, C.: Simulation von chemischen Tracern mit ICON-ART, Master's thesis, Karlsruhe Institute of Technology (KIT), Germany, 2015.

Suzuki, K., Nakajima, T., Satoh, M., Tomita, H., Takemura, T., Nakajima, T. Y., and Stephens, G. L.: Global cloud-system-resolving simulation of aerosol effect on warm clouds, Geophys. Res. Lett., 35, doi:10.1029/2008GL035449, l19817, 2008.

van der Werf, G. R., Randerson, J. T., Giglio, L., Collatz, G. J., Kasibhatla, P. S., and Arellano Jr., A. F.: Interannual variability in global biomass burning emissions from 1997 to 2004, Atmos. Chem. Phys., 6, 3423–3441, doi:10.5194/acp-6-3423-2006, 2006.

van der Werf, G. R., Randerson, J. T., Giglio, L., Collatz, G. J., Mu, M., Kasibhatla, P. S., Morton, D. C., DeFries, R. S., Jin, Y., and van Leeuwen, T. T.: Global fire emissions and the contribution of deforestation, savanna, forest, agricultural, and peat fires (1997-2009), Atmos. Chem. Phys., 10, 11 707–11 735, doi:10.5194/acp-10-11707-2010, 2010.

Vogel, B., Vogel, H., Bäumer, D., Bangert, M., Lundgren, K., Rinke, R., and Stanelle, T.: The comprehensive model system COSMO-ART - Radiative impact of aerosol on the state of the atmosphere on the regional scale, Atmos. Chem. Phys., 9, 8661–8680, doi:10.5194/acp-9-8661-2009, 2009.

Wan, H., Giorgetta, M. A., Zängl, G., Restelli, M., Majewski, D., Bonaventura, L., Fröhlich, K., Reinert, D., Rípodas, P., Kornblueh, L., and Förstner, J.: The ICON-1.2 hydrostatic atmospheric dynamical core on triangular grids - Part 1: Formulation and performance of the baseline version, Geosci. Model Dev., 6, 735–763, doi:10.5194/gmd-6-735-2013, 2013.

Williams, J., van Velthoven, P., and Brenninkmeijer, C.: Quantifying the uncertainty in simulating global tropospheric composition due to the variability in global emission estimates of Biogenic Volatile Organic Compounds, Atmos. Chem. Phys., 13, 2857–2891, doi:10.5194/acp-13-3693-2013, 2013.

World Meteorological Organization (WMO): Meteorology: A Three-Dimensional Science: Second Session of the Commission for Aerology, WMO Bulletin IV, WMO, Geneva, 1957.

Zängl, G., Reinert, D., Rípodas, P., and Baldauf, M.: The ICON (ICOsahedral Non-hydrostatic) modelling framework of DWD and MPI-M: Description of the non-hydrostatic dynamical core, Quart. J. Roy. Meteor. Soc., 141, 563–579, doi:10.1002/qj.2378, 2015.